Journal of Engineering and Technology Research

Volume 6 Number 7 November 2014
ISSN 2006-9790

Academic Journals

ABOUT JETR

The **Journal of Engineering and Technology Research (JETR)** is published monthly (one volume per year) by Academic Journals.

Journal of Engineering and Technology Research (JETR) is an open access journal that provides rapid publication (monthly) of articles in all areas of the subject such as Artificial Intelligence Applications and Innovations, Information Systems, Kinetic Processes in Materials, strength of building materials, engineering applications for world problems etc.
The Journal welcomes the submission of manuscripts that meet the general criteria of significance and scientific excellence. Papers will be published shortly after acceptance. All articles published in JETR are peer-reviewed.

Contact Us

Editorial Office: jetr@academicjournals.org

Help Desk: helpdesk@academicjournals.org

Website: http://www.academicjournals.org/journal/JETR

Submit manuscript online http://ms.academicjournals.me/

Editorial Board

Journal of Engineering and Technology Research

Table of Content: Volume 6 Number 7 November 2014

ARTICLES

Research Articles

academicJournals

Vol. 6(6), pp. 94-106, November 2014
DOI: 10.5897/JETR2014.0382
Article Number: 887FD9648279
ISSN 2006-9790

http://www.academicjournals.org/JETR

Journal of Engineering and Technology Research

Full Length Research Paper

Analysis and parametric optimization of flux cored arc welding process for IS 2062 mild steel plates using Taguchi method and utility concept

P. Sreeraj[1]*, T. Kannan[2] and S. Maji[3]

[1]Department of Mechanical Engineering, Younus College of Engineering and Technology, Kerala, 691010 India.
[2]SVS College of Engineering, Coimbatore, Tamilnadu, 642109 India.
[3]Department of Mechanical Engineering, IGNOU, Delhi, 110068, India.

Received 19 June, 2014; Accepted 29 September, 2014

Optimization of flux cored arc welding (FCAW) process parameters were carried out to obtain optimum weld bead geometry in mild steel plates of IS 2062 by using an alternate Taguchi method. Design of experiments based on multi-objective Taguchi approach was employed for development of mathematical model correlating important process parameters like welding voltage (V), welding current (I), stick out (N) and wire speed (T), with weld bead parameters like penetration (P) and percentage of dilution as responses. The optimum welding parameters were investigated using Taguchi method with L_{16} orthogonal array (OA). The developed models have checked for adequacy and significance based on analysis of variance (ANOVA) test. Because of high reliability, easiness in operation, high penetration good surface finish and high productivity FCAW became a natural choice for fabrication industries. Based on confirmation test, the proposed model can be effectively used to optimize the welding performance. The utility concept was used for optimization of bead geometry and results are presented.

Key words: Flux cored arc welding (FCAW), optimization, analysis of variance (ANOVA), Taguchi approach, utility concept.

INTRODUCTION

Quality is a vital factor in today's manufacturing world. Quality can be defined as the degree of customer satisfaction. Quality of a product depends on how it performs in desired circumstances. Quality is avery vital factor in the field of welding. The quality of a weld depends on mechanical properties of the weld metal which in turn depends on metallurgical characteristics and chemical composition of the weld. The mechanical and metallurgical feature of weld depends on bead geometry which is directly related to welding process parameters. In other words, quality of weld depends on in process parameters. Flux cored arc welding (FCAW) welding is a multi-objective and multifactor metal fabrication technique. The process parameters have a direct influence on bead geometry.

Figure 1 shows the weld bead geometry. Mechanical strength of weld metal is highly influenced by the composition of metal but also by weld bead shape.

*Corresponding author. E-mail: pathiyasseril@yahoo.com

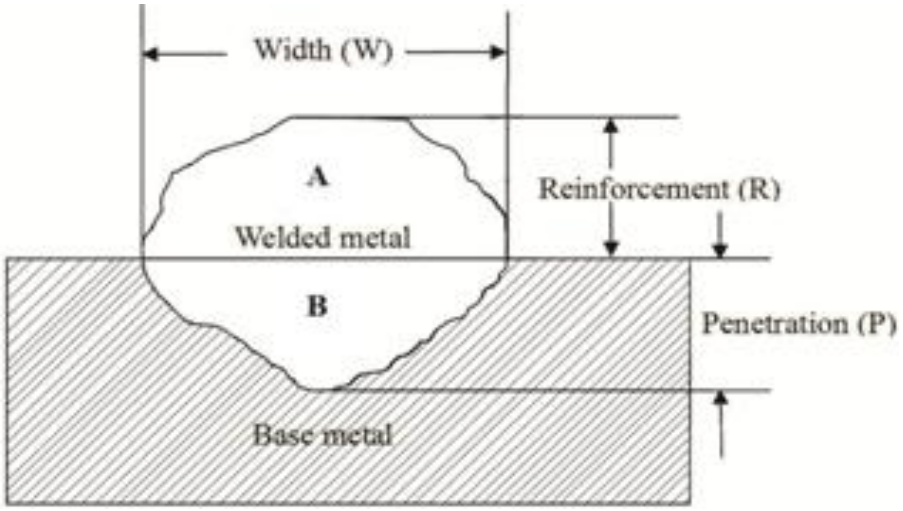

Figure 1. Weld bead geometry. Percentage dilution (D) = [B / (A + B)] × 100.

(Kannan et al., 2013). This is an indication of bead geo geometry. It mainly depends on wire speed, welding current, voltage and stick out etc. Therefore, it is necessary to study the relationship between in process parameters and bead parameters to study weld bead geometry (Lijo and Somashekher, 2013). This paper highlights the study carried out to develop mathematical models to optimize weld bead geometry, in bead on plate welding deposited by FCAW.

The multi characteristics optimization model based on Taguchi method and utility concept has been employed to determine the optimal combination of welding parameters to attain minimum percentage of dilution and maximum penetration simultaneously. The confirmation test was also conducted to verify the results.

TAGUCHI METHOD

Taguchi method uses a special type of design of orthogonal arrays (OA) to study the entire parameter space with smaller number of experiments. The OA is a small set from all possibilities which helps to determine the least number of experiments, which will further helps to determine the optimum level for each process parameters and establish the relative importance on individual process parameters. Appropriate selection of OA is the first step of Taguchi approach. The minimum number of experimental trials performed in an OA is given by N_{min} = (L-1) F + 1; where F is the number of factors and L is the number of levels. Taguchi method utilizes a statistical measure of performance called signal-to-noise (S/N) ratio. The ratio depends on the quality characteristics of product/process to be optimized. The experimental results are then transferred to S/N ratio. This ratio can be used to measure the quality characteristics deviating from desired values. Usually, there are three categories in the analysis of the S/N ratio, that is, the lower-the-better, higher-the-better and nominal-the-better. Regardless of category of quality characteristics larger S/N ratio corresponds to the better quality characteristics (Jagannatha et al., 2012). The optimal process parameters are the levels with highest S/N ratio. Analysis of variance (ANOVA) tests are performed to see that the process parameters are statically significant. Finally, a confirmation experimented is conducted to verify the optimal process parameters.

The multi-response methodology based on Taguchi's robust design technique and utility concept was used for optimizing the multi responses like dilution and penetration. Taguchi's standard S/N ratios were selected to obtain the optimum parameters. They were the larger-the-better type for penetration and dilution as calculated by Equation 1, and Equation 2 represents smaller-the-better type, respectively.

$$\eta = -10log_{10}\left|\frac{1}{p^2}\right| \quad (1)$$

$$\eta = -10log_{10}|D^2| \quad (2)$$

UTILITY CONCEPT

Welding process is a multi-factor multi-objective problem; the optimum solution is a compromise. The models developed were used for optimization of FCAW process parameters to obtain good bead geometry. Utility can be defined as the usefulness of a product or service into the levels of expectations to the consumers. The usefulness of a process can be represented by a unified index termed as utility which is the summation of the individual utilities of various quality characteristics (Norasiah et al., 2012). It is difficult to obtain the best combination process parameters, when there are multi responses to be optimized. If x_i represents the measure of effectiveness and n represents the number of responses, then overall utility function can be defined as:

$$U(x_1, x_2.....x_n) = f[U_1(x_1), U_2(x_2).....U_n(x_n)] \quad (3)$$

Where $U(x_1, x_2.....x_n)$ is the overall utility of n process response characteristics and $U_1(x_1)$ is the utility of I_{th} response. Assignment of weights is based on the requirements and priorities among the various responses. Therefore, weighted form can be expresses as:

Table 1. Chemical composition of base metal and filler wire.

	Elements weight (%)								
Material	**C**	**SI**	**Mn**	**P**	**S**	**Al**	**Cr**	**Mo**	**Ni**
IS 2062	0.150	0.160	0.870	0.015	0.016	0.031	-	-	-
E7 IT- 1C	1.12	0.90	1.75	0.030	0.030	-		0.30	0.50

Table 2. Welding parameters and their levels.

Parameter	**Factor levels**					
	Unit	**Notation**	**1**	**2**	**3**	**4**
Welding voltage	V	V	20	22	24	25
Welding current	A	I	87	123	138	155
Stick out	mm	N	15	20	25	30
Wire speed	mm/min	T	25	40	50	53

$$U(x_1, x_2.....x_n) = \sum_{i=1}^{n} WiUi(Xi) \quad (4)$$

Where $\sum_{i=1}^{n} Wi = 1$

Where W_i is the weight assigned to *i* th response. The utility concept employs the weighing factors to each S/N ratio for each trial and multi response S/N ratio calculated using Equation 5:

$$\eta = \eta_1 W_1 + \eta_2 W_2 \quad (5)$$

Where W_1 and W_2 are the weight factors associated with S/N ratios. It is taken as 0.5. The overall mean of η associated with *k* number of trials is computed as:

$$M = \frac{1}{k} \sum_{1}^{n} \eta k \quad (6)$$

These weighing factors are determined based on priorities among the various responses to be simultaneously optimized. In this experimental work, it is taken as 0.5. This gives priorities to all the responses for simultaneous maximization and minimization (Cochran and Coxz, 1987). The overall mean of η associated with *k* number of trials is computed from Equation 6.

EXPERIMENTATION

Test plates of size 300 × 200 × 6 mm were cut from mild steel plate of grade IS - 2062 and one of the surfaces is cleaned to remove oxide and dirt before welding. E7 IT-1C wire of 1.2 mm diameter was used for bead on plate welding. The properties of base metal and filler wire are shown in Table 1.

The selection of the welding electrode wire was based on the matching, the mechanical properties and physical characteristics of the base metal, weld size and existing electrode inventory (Norasiah et al., 2012). These have good surface appearance, good radiographic standard quality and minimum electrode wastage.

PLAN OF INVESTIGATION

The research work is carried out in the following steps (Tarng and Yang, 1998): Identification of factors, finding the limit of process variables, development of OA, conducting experiments as per OA, recording responses, development of mathematical models and checking adequacy of developed models. Utility concept applied further for optimization.

Identification of factors and responses

The percentage of dilution has got an important influence in welding. The properties of the welding are significantly influenced by dilution obtained. Hence, control of dilution is important in welding where a high dilution is highly desirable. When dilution is quite low, the final deposit composition will be closer to that of filler material and hence corrosion resistant properties of welding will be greatly improved. The chosen factors have been selected on the basis to get optimal dilution and optimal weld bead geometry (Kannan et al., 2013). These are wire speed rate (T), welding voltage (V), welding current (I) and stick out (N). The responses chosen were depth of penetration (P) and percentage of dilution (D). The responses were chosen based on the impact of parameters on final composite model.

Finding the limits of process variables

Working ranges of all selected factors are fixed by conducting trial run. This was carried out by varying one of the factors while keeping the rest of them as constant values. Working range of each process parameters was decided upon by inspecting the bead for smooth appearance without any visible defects. The chosen level of the parameters with their units and notation are given in Table 2.

Development of orthogonal array

In full factorial design, number of experimental runs may be high. This results increase in cost and time. In order to avoid this,

Table 3. Design matrix and observed values of weld bead geometry.

Trial No.	Design matrix				Bead parameter	
	V	I	N	T	P (mm)	D (%)
1	1	1	1	1	1.235	17.623
2	1	2	2	2	1.347	17.462
3	1	3	3	3	1.388	17.842
4	1	4	4	4	1.425	17.442
5	2	1	2	3	1.657	18.332
6	2	2	1	4	1.586	16.692
7	2	3	4	1	1.456	17.823
8	2	4	3	2	1.738	20.424
9	3	1	3	4	1.416	17.912
10	3	2	4	3	1.537	18.182
11	3	3	1	2	1.465	18.218
12	3	4	2	1	1.368	17.512
13	4	1	4	2	1.487	18.221
14	4	2	3	1	1.398	17.943
15	4	3	2	4	1.457	17.841
16	4	4	1	3	1.868	21.512

P, Penetration; D, dilution %.

Taguchi's L_{16} (4^4) OA consisting 16 sets of data has been selected to optimize the experimental data. This is shown in Table 3.

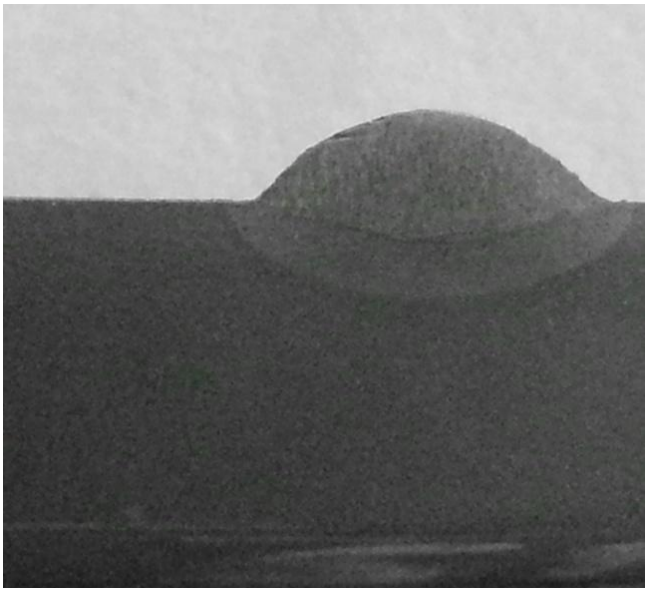

Figure 2. Welded specimen

Conducting experiments as per orthogonal array

In this work, 16 experimental runs were allowed as per the OA as shown Table 3 at random (Saurav et al., 2008). At each run settings, all parameters were disturbed and reset for next deposit. This is very essential to introduce variability caused by errors in experimental set up.

Recording of responses

For measuring the clad bead geometry, the transverse section of each weld overlays was cut using band saw from mid length. Position of the weld and end faces were machined and grinded. The specimen and faces were polished and etched using a 5% nital solution to display bead dimensions. The weld bead profiles were traced using a reflective type optical profile projector at a magnification of ×10 (Gunaraj and Murugan, 1999). Then the bead dimension such as depth of penetration and dilution were measured (Montgomery, 2003). The profiles traced using AUTO CAD software. The welded specimen is shown in Figure 2 (Kannan and Yoganath, 2010; Dawei et al., 2013). The measured weld bead dimensions and percentage of dilution is shown in Table 3.

RESULTS AND DISCUSSION

Analysis of single response

Experiments were conducted on IS 2062 mild steel plate to study the performance of bead on plate welding using the FCAW method by L_{16} OA. The values of single response S/N ratios of penetration and dilution are calculated using larger-the-better criteria, calculated using Equation 1. The combined multi-response S/N ratio is calculated using Equation 5, respectively. The individual values of S/N ratios are shown in Table 6. It can be found that the optimal combination of $V_2I_4N_1T_3$ is

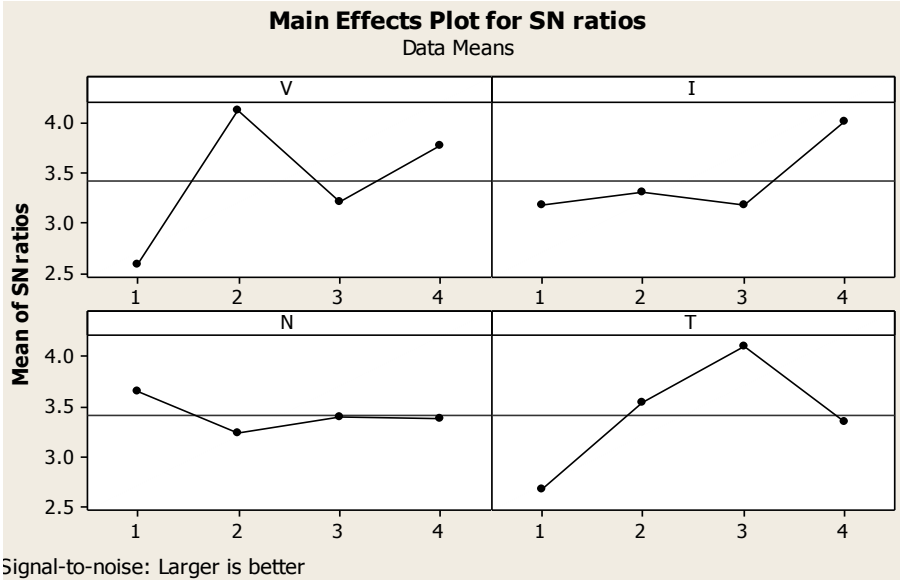

Figure 3. Main effects of plots based on S/N ratio of penetration.

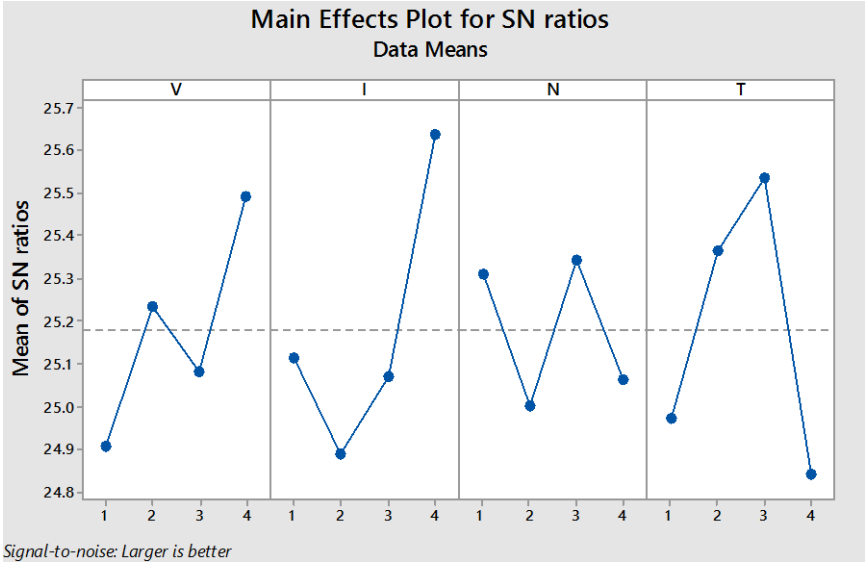

Figure 4. Main effects of plots based on S/N ratio of dilution.

the largest value of S/N ratio of penetration and for dilution it is $V_4I_4N_1T_3$, respectively. Therefore, $V_2I_4N_1T_3$ is the optimal combination of responses for penetration and for dilution $V_4I_4N_1T_3$ is the optimal combination. The main effect plots (Figures 3 and 4) shows that the optimum condition for penetration and dilution are at level, 22 V, 155 Amps, 15 mm and 53 mm/min for penetration 25V, 155 Amps, 15 mm and 53 mm/min, respectively. Table 4 and 6 show the response table for signal to noise ratios for penetration and dilution.

The statistical software MINITAB 15 is used to determine the ANOVA. The purpose of ANOVA is to investigate which welding parameter significantly affects the performance contribution. In addition, F-test was used to determine which welding factor has significant effect on performance. When F value is large then that factor has significant effect on performance. The results of ANOVA for single-response S/N ratio of dilution and penetration are shown in Tables 5 and 7, respectively. It can be seen that welding current has highest contribution

Table 4. Response table for signal to noise ratios penetration.

Level	V	I	N	T
1	2.586	3.172	3.646	2.682
2	4.114	3.072	3.241	3.538
3	3.198	3.174	3.395	4.099
4	3.763	4.007	3.380	3.343
Delta	1.528	0.835	0.405	1.417
Rank	1	3	42	

Table 5. ANOVA for penetration.

Source	DF	Seq SS	Adj SS	Adj MS	F	P
V	3	0.036551	0.036551	0.0365512	1.55965	0.237640
I	3	0.005056	0.005056	0.0050562	0.21575	0.651356
N	3	0.035870	0.035870	0.0358705	1.53060	0.241782
T	3	0.040230	0.040230	0.0402304	1.71664	0.216825
Error	3	0.257791	0.257791	0.0234355		
Total	15	0.375499				

Table 6. Response table for signal to noise ratios on dilution.

Level	V	I	N	T
1	24.91	25.12	25.31	24.97
2	25.23	24.89	25.00	25.37
3	25.08	25.07	25.34	25.53
4	25.49	25.64	25.06	24.84
Delta	0.59	0.75	0.34	0.69
Rank	3	1	4	2

of about 65.1% for penetration and stick out with 69.7.7% contribution for dilution. The other parameters have less contribution. It is clear that the welding current and stick out are one of the significant factors that has more impact than any other factors on dilution and penetration.

Optimal parameter combination of Multi response

The optimal combination of process parameters for simultaneous optimization of dilution and penetration is obtained by means of values of multi-responses S/N ratio of overall utility and is shown in Table 8.

The larger values of multi-responses S/N ratio means the comparable sequence exhibiting a stronger correlation with the reference sequence. Based on the study, combination of $V_2I_4N_1T_3$ shows the largest values of multi-response S/N ratio for the factors V, I, N and T, respectively. Therefore, $V_2I_4N_1T_3$ is the optimal parameter combination of flux cored arc bead on plate welding for IS 2062 steel plates, which are shown in Figure 5. Table 9 shows the response table for multi-response signal to noise ratios.

The results of ANOVA for multi-response S/N ratio are shown in Table 10. On examining the percentage of contribution (P %) of different factors, it can be seen that welding current is about 34.7% and other parameters have significant contributions. It is clear that welding current is one of the significant factors that have more impact than any other factors. The main effect plot, (Figure 5), shows that optimum condition for multiple responses is/are at level, 22 V, 155 Amps, 15 mm and 53 mm/min, respectively.

Confirmation test

The final step is the verification experiments to validate

Table 7. Analysis of variance for dilution.

Source	DF	Adj SS	Adj MS	F	P
Regression	4	5.8337	1.45843	1.08	0.412
V	1	2.4490	2.44895	1.81	0.205
I	1	3.1407	3.14068	2.33	0.155
N	1	0.2160	0.21601	0.16	0.697
t	1	0.0281	0.02809	0.02	0.888
Error	11	14.8450	1.34955		
Total	15	20.6787			

Table 8. S/N ratios of penetration and dilution and multi response.

S/N ratio D (%)	S/N ratio P	S/N ratio multi response
24.9216	1.83334	13.37747
24.8419	2.58735	13.71463
25.0289	2.84779	13.93835
24.8319	3.07630	13.9541
25.2642	4.38645	14.82533
24.4502	4.00606	14.22813
25.0196	3.26323	14.14142
26.2028	4.80100	15.5019
25.0629	3.02127	14.04209
25.1928	3.73348	14.46314
25.2100	3.31675	14.26338
24.8667	2.72172	13.79421
25.2114	3.44622	14.32881
25.0779	2.91014	13.99402
25.0284	3.26919	14.1488
26.6536	5.42754	16.04057

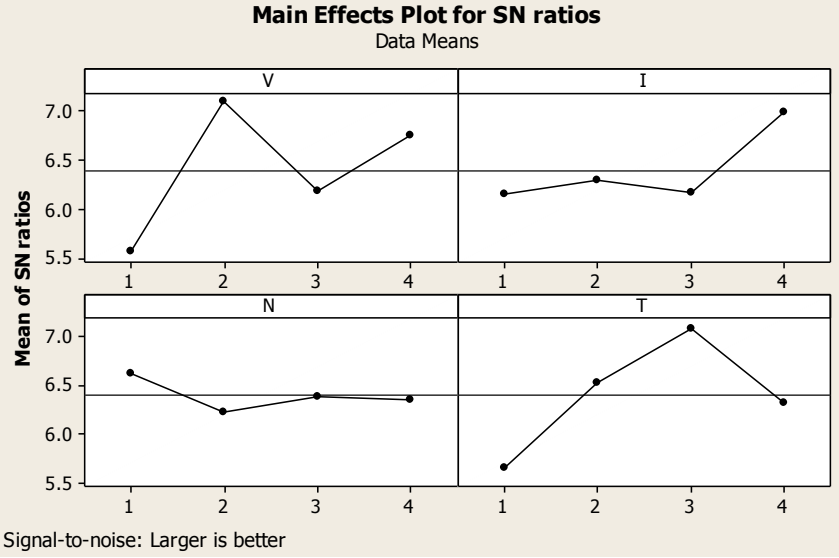

Figure 5. Main effect of plots based on S/N ratios multiple responses.

Table 9. Response table for multi-response S/N ratios.

Level	I	S	N	T
1	5.571	6.154	6.626	5.667
2	7.091	6.289	6.222	6.520
3	6.181	6.157	6.378	7.078
4	6.744	6.987	6.361	6.323
Delta	1.520	0.833	0.404	1.411
Rank	1	3	4	2

Table 10. Analysis of variance for multi response S/N ratios.

Source	DF	Seq SS	Adj SS	Adj MS	F	P
V	3	5.3253	5.3253	1.77510	25.82	0.012
I	3	0.3385	0.3385	0.11568	1.64	0.347
N	3	1.9070	1.9070	0.63658	9.25	0.050
T	3	4.0699	4.0699	1.35664	19.73	0.018
Error	3	0.2063	0.2063	0.06876		
Total	15	11.8470				

Table 11. Results of confirmation tests

Level	Performance Characteristic	Optimal setting	Predicted S/N ratio	Experimental S/N ratio
SRO	Penetration (P)	$V_2I_4N_1T3$	5.4275	7.5062
	Dilution (D)	$V_4I_4N_1T_3$	13.7874	14.7424
MRO	P and D	$V_2I_4N_1T_3$	16.0405	17.7646

optimum conditions suggested by the matrix experiments which indeed give the projected experiment. Confirmation experiments is performed by conducting a test with a specific combination of factors and levels previously evaluated. After determining the optimum conditions new experiment was conducted with optimum levels. Then predicted parameters were calculated using Equation 7.

$$\eta\_opt = \bar{\eta} + \sum_{i=1}^{p} \eta_{mi} - \bar{\eta} \quad (7)$$

Where m is the total mean of the responses S/N ratio at the optimal level and m_i is the S/N ratio at the optimal parameter. The predicted optimal values of single and multi-response function are shown in Table 11. The improvement in S/N ratio is found. So there is considerable improvement in quality with multi-response function.

In order to validate the experiment, four trials are conducted according to the optimal parameters level, $V_2I_4N_1T_3$ and corresponding values of performance measures are taken. Table 11 shows the predicted multi-response S/N ratio and multi-response S/N ratio obtained from experiment. It may be noted that there is a good agreement between estimated value (16.0405) and the experiment (17.7646). Therefore, the condition $V_2I_4N_1T_3$ is treated as optimal. The optimal condition, $V_2I_4N_1T_3$, (22 V, 155 Amps, 15 mm and 53 mm/min) is confirmed by ANOVA.

Conclusions

Optimization of process parameters of FCAW has been carried out using Taguchi's OA with multi response analysis as discussed in this paper. From the analysis, the following conclusions have been drawn:

1) It has been found that the combination $V_2I_4N_1T_3$ show the largest values of multi-response S/N ratio for factors V, I, N and T. Therefore, $V_2I_4N_1T_3$ is optimal parameter combination with voltage, current, stick out and wire feed

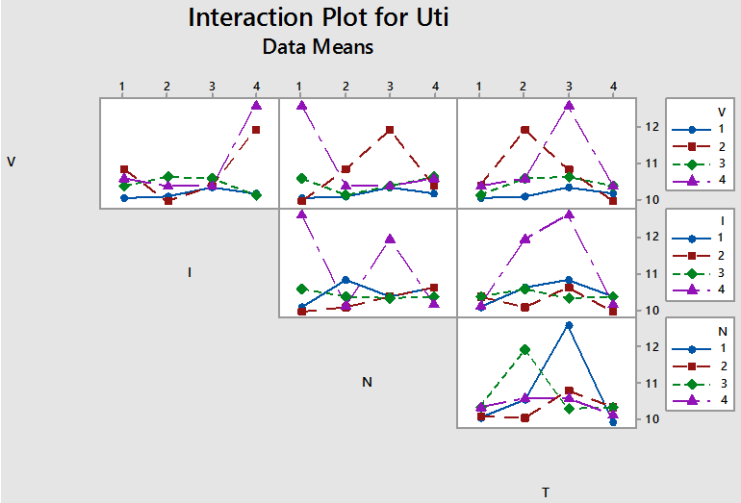

Figure 6. Interaction plot for multi-response.

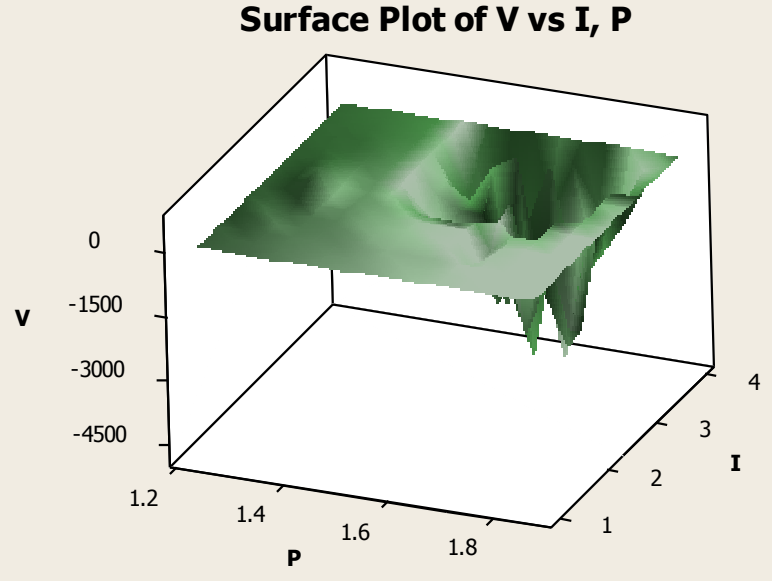

Figure 7. Interaction effect of voltage and current on penetration.

of the flux cored bead on plate welding on IS 2022 mild steel plates.

2) Through ANOVA, percentage of contribution to the stick out is more as compared to other parameters. Hence, the most significant factor for the flux cored bead on plate welding for maximization of dilution and maximization of penetration is stick out.

3) It can be found that there is a good agreement between estimated and experimental value. Therefore, in this welding process $V_2I_4N_1T_3$ is treated as optimum parameter combination.

4) From the experimental results, it can be found that welding current and stick out has largest impact on dilution and penetration.

5) Figure 6 illustrates the interaction effects of process parameters for multi-response optimization. It is observed that if the lines are parallel and not over lapping there is little or no evidence of an interaction in the parameters.

6) Figure 7 shows the interaction effects of voltage and current on penetration. Figure 8 shows surface plot voltage and current on dilution.

7) Figure 9 shows combination of process parameters with penetration.

8) Figures 10 to 13 show microstructures of various

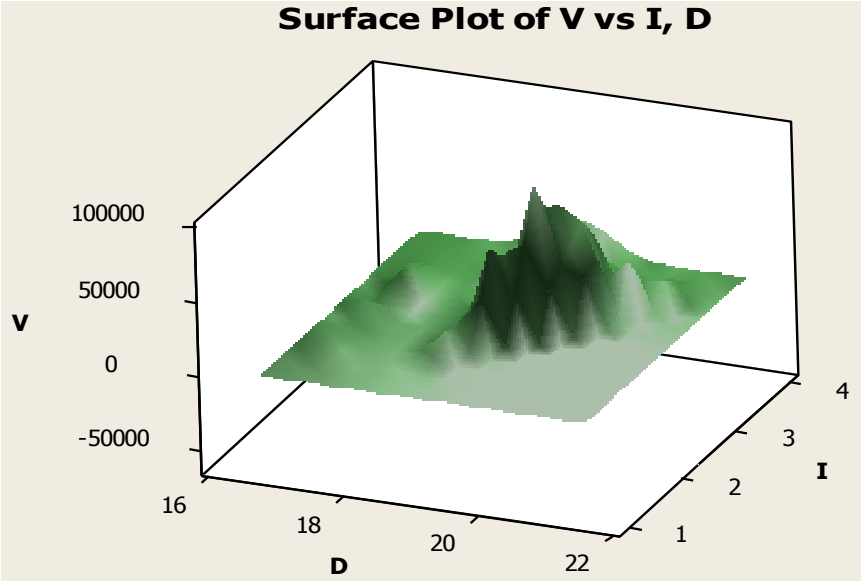

Figure 8. Interaction effects of voltage and current on dilution.

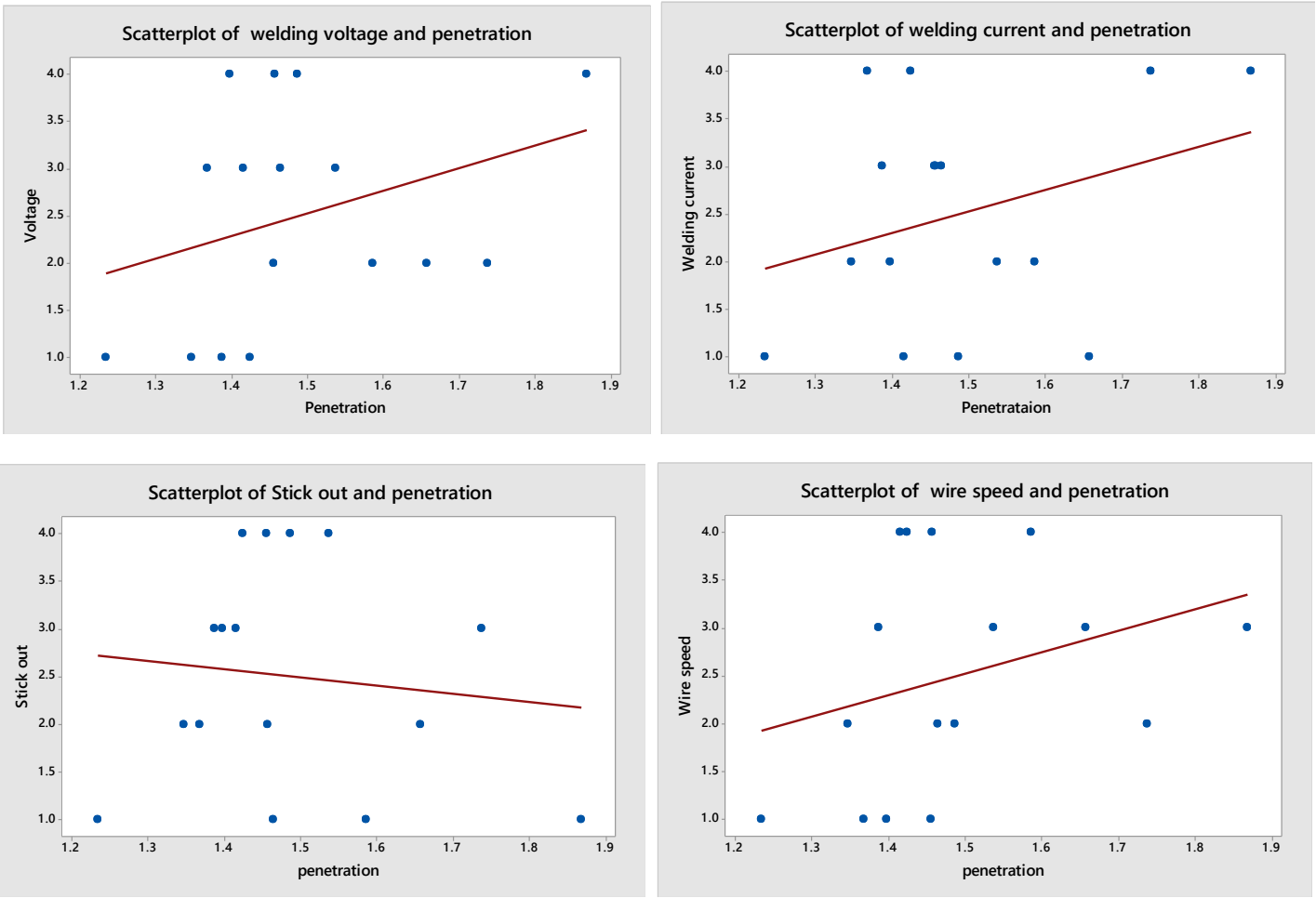

Figure 9. Combination of process parameters and penetration.

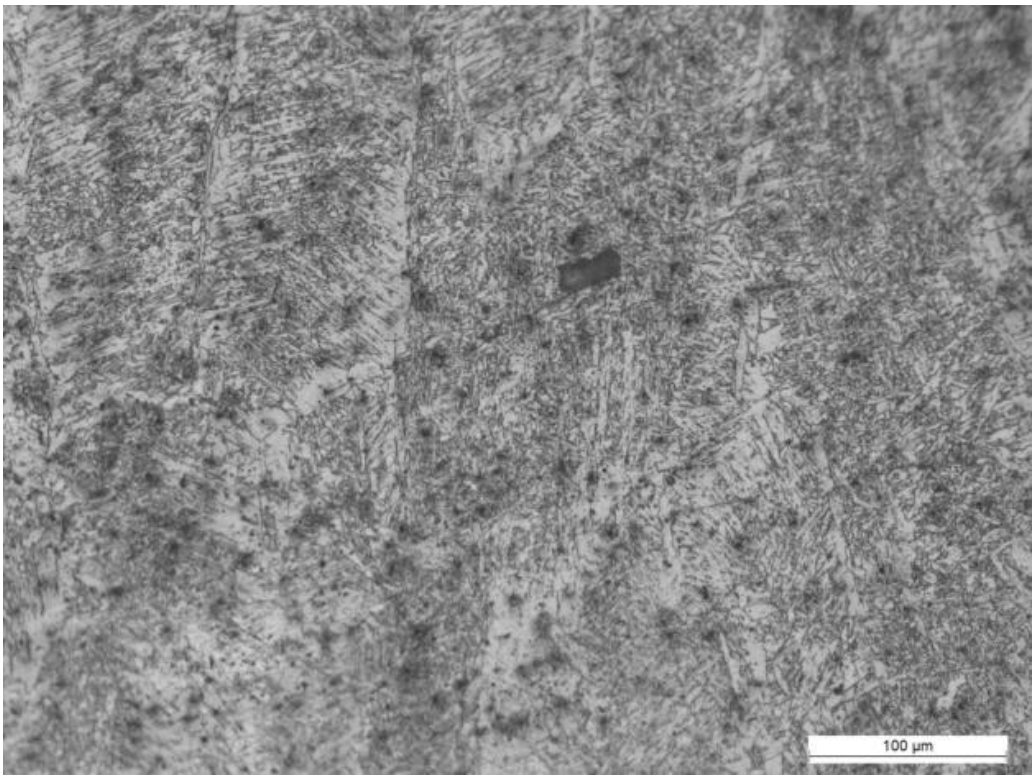

Figure 10. Microstructure of HAZ.

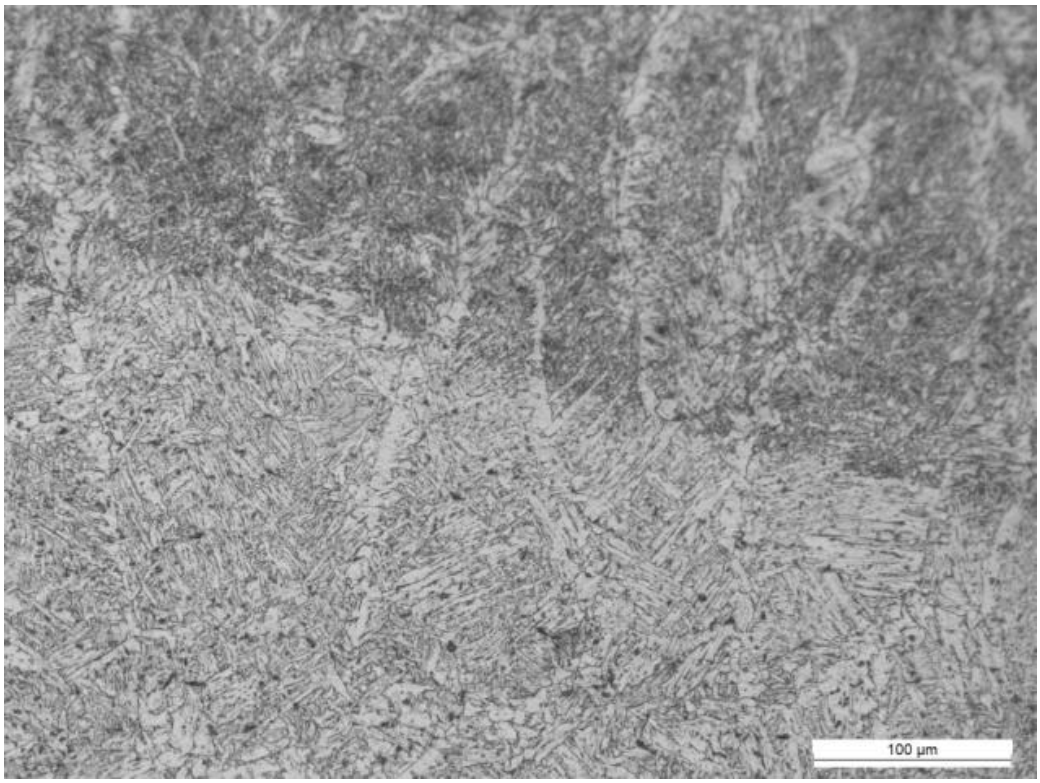

Figure 11. Microstructure of fusion line.

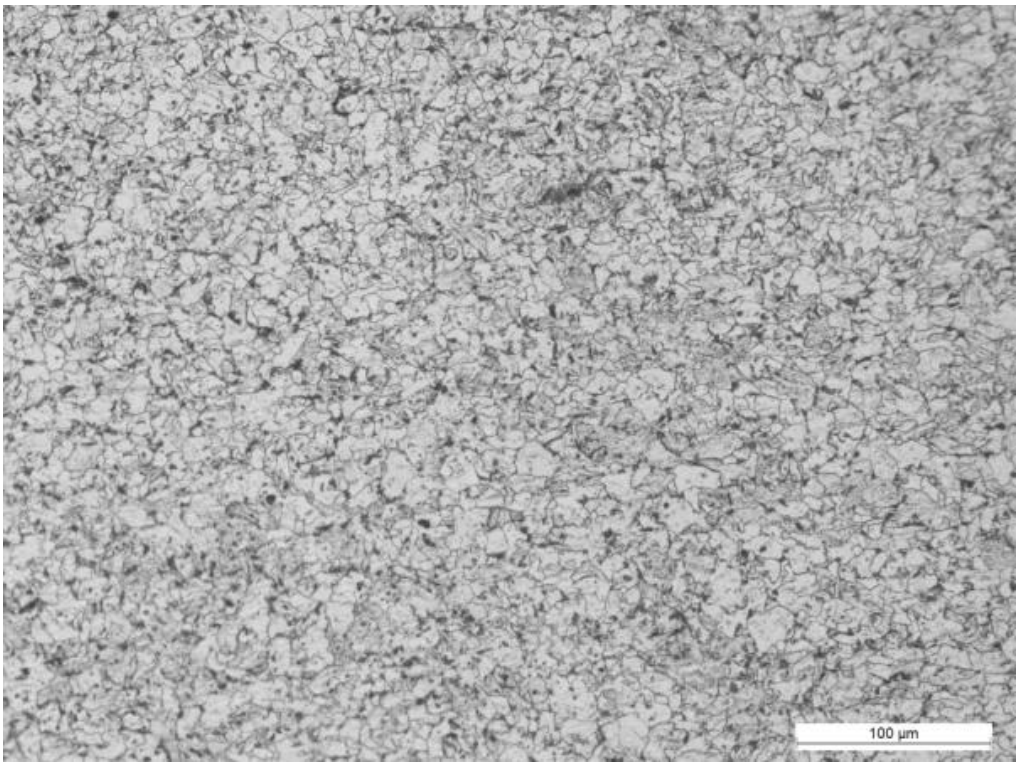

Figure 12. Microstructure of weld zone.

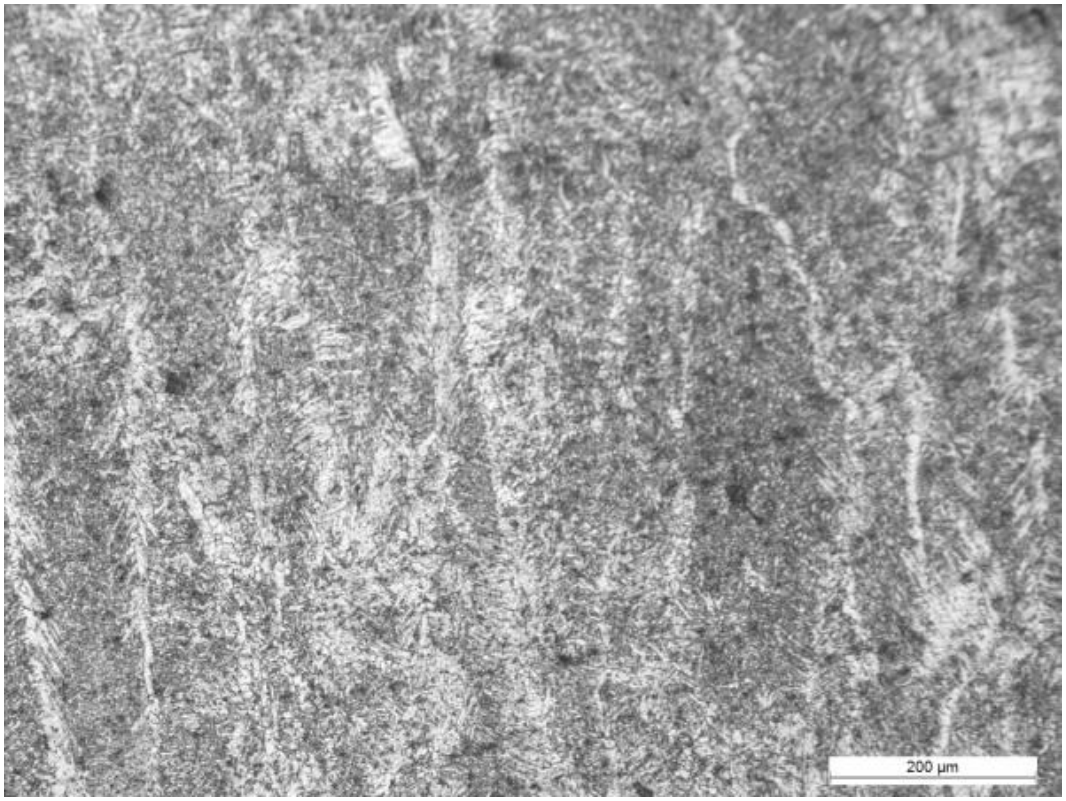

Figure 13. Microstructure of HAZ.

welding zones of specimens. From the microstructure figures, it can be seen that in the weld zone the grain structure is somewhat fine. In HAZ, it is somewhat coarse this is due to dendrite formation.

Conflict of Interest

The author(s) have not declared any conflict of interest.

ACKNOWLEDGEMENT

The authors sincerely acknowledge the help and facilities extended to them by the Department of Mechanical Engineering, Younus College of Engineering and Technology, Kollam, India.

Conflict of Interest

The authors have not declared any conflict of interest.

REFERENCES

Cochran WG, Coxz GM (1987). Experimental Design., New York, John Wiley & Sons. P. 370.

Dawei Z, Yuanxun W, Suning S, Zongguo L (2013). Multi objective optimal design of small scale resistance spot welding process with principal component analysis and response surface methodology. J. intell. manuf. DOI,10.1007/s10845-013-0733-2.

Gunaraj V, Murugan N (1999). Prediction and comparison of the area of the heat effected zone for the bead on plate and bead on joint in SAW of pipes, J. Mater. Process. Technol. 95:246-261.

Kannan TY (2010). Effect of process parameters on clad bead geometry and shape relationships of stainless steel cladding deposited by GMAW. Int. J. Manuf. Technol. 47:1083-1095.

Kannan T, Murugan N, Sreeharan BN (2013). Optimization of flux cored arc welding process parameter using genetic and memetic algorithms. J. Manuf. Sci. Prod. 13(4):239-250.

Jagannatha N, Hiremath SS, Sadashivappa K (2012). Analysis and parametric optimization of abrasive hot air jet machining for glass using Taguchi method and utility concept. Int. J. Mech. Mater. Eng. 7(1):9–15.

Montgomery DC (2003). Design and analysis of Experiments, John Wiley & Sons (ASIA) Pvt. Ltd.

Norasiah M, Manurung Y, Hafidzi M, Abas S, Tham G, Haruman E (2012). Optimization and modelling of spot welding parameters with simultaneous response consideration using multi objective Taguchi method and utility concept. J. Mech. Sci. Technol. 26(8):2365-2370.

Saurav D, Ashish B, Pradip KP (2008). Grey based Taguchi method for optimization of bead geometry in submerged arc bead on plate welding. Int. J. Adv. Manuf. Technol. 39:1136-1143.

Somashekher L, Hiremath S (2013). Response surface modelling of micro holes in electro chemical discharge machining process. Proceed Engr. 64:1335-1404.

Tarng YS, Yang WH (1998) Optimization of weld bead geometry in gas tungsten arc welding by the Taguchi method. Int. J. Adv. Manuf. Technol. 14:549-554.

academicJournals

Vol. 6(7), pp. 107-114, November 2014
DOI: 10.5897/JETR2013.0332
Article Number:ED7FC6848284
ISSN 2006-9790

http://www.academicjournals.org/JETR

Journal of Engineering and Technology Research

Full Length Research Paper

New technique based on uterine electromyography nonlinearity for preterm delivery detection

Safaa M. Naeem*, Ahmed F. Seddik and Mohamed A. Eldosoky

Department of Biomedical Engineering, Helwan University, Helwan, Egypt.

Received 3 October, 2013; Accepted 29 September, 2014

Detecting uterine electromyography (EMG) signals can yield a promising approach to determine and take actions to prevent preterm deliveries. This paper objective is to predict this risk using such uterine signals. Previous classification studies have used only linear signal processing which depends on the spectral characteristics of the uterine EMG signals that did not give clinically acceptable results. On the other hand some studies have made linear and non-linear analysis for the signals and have found that the non-linear parameters can distinguish the preterm delivery in better way than the linear parameters. In this research, two methods will be taken; the first method is to take some linear parameters to a suitable neural network and the second one is to take some non-linear parameters to the same network. Then, the two results are compared by calculating parameters False Positive Rate, False Negative Rate, True Positive Rate, True Negative Rate and Accuracy to evaluate the classification performance. Besides, a linear parameter, discrete cosine transform, which depends on the spectral characteristics of the signals, is taken as an additional feature to the same network so the research will have a third method to illustrate the difference between the traditional previous classification method and the proposed ones. Applying the second method gives better results than the first and the third methods. The paper can propose a method depends on the uterine EMG nonlinearity which gives best results to detect preterm delivery compared with those used in previous studies.

Key words: Uterine electromyography (EMG) signals, term-preterm deliveries prediction, neural network performance evaluation, discrete cosine transform.

INTRODUCTION

A most urgent challenge in healthcare currently is the phenomenon of preterm labor, or labor prior to 37 completed weeks of gestation. Preterm labor leaves serious impacts on economy and society as a whole. The complications of preterm birth include significant neurological, mental, behavioral and pulmonary problems in later child's life (Diab et al., 2010). So any promising technique that could improve the chances of preterm birth prediction is required. Analysis of uterine electromyography (EMG), termed as electrohysterogram (EHG), records is one such technique.

Uterine EMG has been the subject of research for many years from 1950. The uterine EMG has been proved to be of interest for pregnancy and parturition

*Corresponding author. E-mail: safaa_naim@h-eng.helwan.edu.eg

monitoring (Diab et al., 2007). Uterine EMG classification, in previous researches, depends on the spectral characteristics of EMG activity. Wavelet transform is a tool that has been used to describe the uterine EMG activity and Power Spectral Density (Diab et al., 2007) as well as the Wavelet Packet Transform (Moslem et al., 2012). Most of the used signal-processing techniques were linear which rely on the changes in the frequency power spectrum of the uterine activity and included the following: the peak frequency of the power spectrum (Garfield et al., 2005); the burst energy levels (Maul et al., 2004); the mean power frequency (Hassan et al., 2010), the use of the peak frequency, the duration and number of bursts, the means and deviations of the frequency spectrum (Maner and Garfield, 2007); and the approaches of analyzing contractions using multiple techniques such as the kurtosis and skewness coefficient. Other approaches included calculating the root mean square of the signals and the median frequency of the power spectrum and the autocorrelation zero-crossing (Fele-Žorž et al., 2008).

It is known that the underlying physiological mechanisms of biological systems are non-linear processes (Akay, 2001). As the uterus is composed of billions of intricately interconnected cells whose responses are non-linear, it may be regarded as a complex, non-linear dynamic system. To analyze the outputs of such a system, non-linear signal processing techniques are applicable. Therefore, one can hypothesize that non-linear signal processing techniques may yield better results in analysis of the EHG than linear ones (Naeem et al., 2013). These techniques included time reversibility and approximate entropy (Hassan et al., 2010), another research estimated Max-Lyapunov exponent, correlation dimension and sample entropy (Fele-Žorž et al., 2008).

In this research, a combination between most of these previous techniques is done as some of the linear techniques and some of non-linear techniques are used in order to estimate their ability to recognize uterine EMG records of term and preterm deliveries using artificial neural networks ANNs.

The following linear features are chosen: the mean power frequency, the root mean square, the peak and median frequencies of the power spectrum and the autocorrelation zero-crossing and taking them into a suitable ANN to calculate the classifier parameters; while the non-linear features are: time reversibility, approximate entropy, the Max-Lyapunov exponent, the correlation dimension, phase space reconstruction based on the derivatives approach and singular spectrum analysis, adjusted amplitude Fourier transform and the sample entropy of the signal and also taking them into the same ANN to calculate the classifier parameters. Finally, compare the results to estimate the ability of linear and non-linear techniques to differentiate uterine EMG records of term and preterm deliveries. It is expectable that the classification method depends on the nonlinear uterine EMG features gives better results.

In addition that, using a linear parameter discrete cosine transform (DCT) which depends on the spectral characteristics and the frequency contents of the uterine EMG signals and is taken as an additional linear feature to the same ANN to illustrate the difference between the traditional previous classification method and the proposed ones. The results show that this method is better than the linear method but the non-linear one is still the best.

MATERIALS AND METHODS

Database description

This research uses Term Preterm ElectroHysteroGram Data Base (TPEHG DB). The records were obtained during regular check-ups either around the 22nd week or around the 32nd week of gestation at the University Medical Centre Ljubljana, Department of Obstetrics and Gynecology, Slovenia (PhysioBank database Website [Online], 2011) and used for studies by Ivan Verdenik (Fele-Žorž et al., 2008). The DB used contains 300 uterine EMG records of which:

(i) 262 records were obtained where delivery was on term
(ii) 143 before the 26th week of gestation.
(iii) 119 during-after the 26th week of gestation.
(iv) -38 records were obtained during pregnancies which ended prematurely
(v) 19 before the 26th week of gestation.
(vi) 19 during-after the 26th week of gestation.

Each record is composed of three channels, recorded from four electrodes as shown in Figure 1. The differences in the electrical potentials of the electrodes produced three channels: S1 = E2–E1, S2 = E2–E3 andS3 = E4–E3.
In this paper, used records were digitally filtered using band pass filter (0.3 to 3 Hz) neglecting either these records were taken after or before the 26th week of gestation but the research uses them generally to make a classification into two classes, term and preterm signals.

Feature extraction

Linear features

Mean power frequency: The mean power frequency (MPF) is the frequency at which the average power within the epoch is reached (Frequency signal analysis-BIOPAC Systems Inc. [Online] (2012) and computed from the power spectral density (PSD) of the signal obtained by Welsh's averaged periodogram method (Hassan et al., 2010).

Peak frequency: The peak frequency is the frequency at which the maximum power occurs during the epoch (Maner and Garfield, 2007). For each signal, *x (t)*, the peak frequency, f_{max}, is calculated as following (Akay, 2001):

$$f_{max} = arg\left(\frac{f_s}{N} max_{i=0}^{N-1} P(i)\right) \quad (1)$$

Where f_s and N denotes the sampling frequency and the number of samples, respectively. P is the frequency-power spectrum.

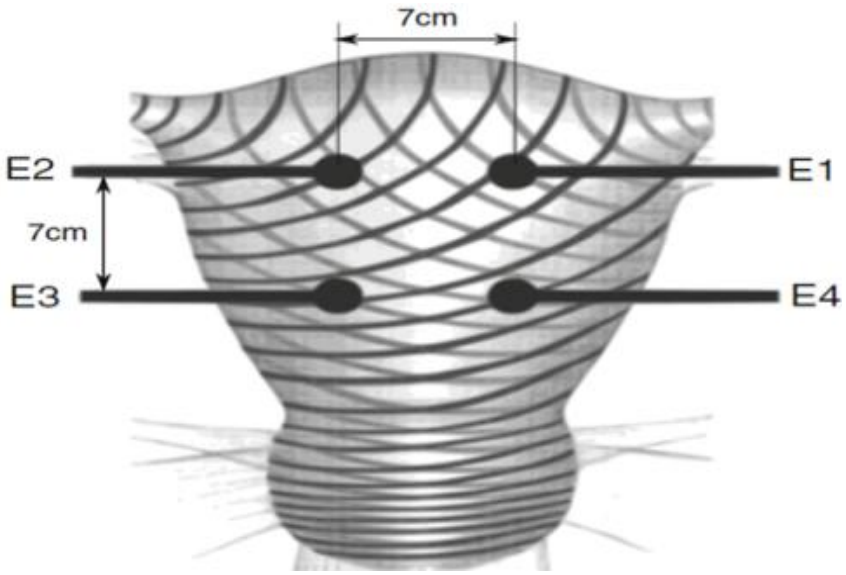

Figure 1. The placement of the electrodes on the abdomen, above the uterine surface.

Root mean square: The root mean square value (RMS) of a signal, *x(i)*, with length *N* is the root of the mean of the squares of all samples in a signal (Fele-Žorž et al., 2008):

$$RMS = \sqrt{\frac{1}{N}\sum_{i=0}^{N-1} x(i)^2} \quad (2)$$

Median frequency: The median frequency was defined as the frequency just above where the sums of the parts above and below in the frequency-power spectrum, *P*, are the same (Fele-Žorž et al., 2008) or it is the frequency at which 50% of the total power within the epoch is reached (Frequency signal analysis-BIOPAC Systems Inc. [Online] (2012).

Autocorrelation zero-crossing: The autocorrelation zero-crossing, τ_{Rxx}, is defined as the first zero-crossing starting at the peak in the autocorrelation, $R_{xx}(\tau)$, of the signal *x(t)* (Fele-Žorž et al., 2008):

$$R_{xx}(\tau_{Rxx}) = 0\,, R_{xx}(\tau) = \sum_{i=0}^{N-1} x(i)\,x(\tau + i) \quad (3)$$

Discrete cosine transform (DCT): DCT generates real spectrum of a real signal and thereby avoids redundant data and computation. The DCT of a real sequence, *x(n)*, with length *N* is defined as:

$$y(k) = w(k)\sum_{n=1}^{N} x(n)\cos\frac{\pi(2n-1)(k-1)}{2N} \quad ,k = 1,..,N \quad (4)$$

$$w(k) = \begin{cases} 1/\sqrt{N} & , \quad k = 1 \\ \sqrt{2/N} & , \quad 2 \le k \le N \end{cases} \quad (5)$$

Non-linear features

Approximate entropy: As mentioned by Pincus (1991) the approximate entropy, ApEn, is defined as a measure that quantifies the regularity and predictability of the signals. The ApEn value is low for regular time series and high for complex, irregular ones (Hassan et al., 2010). This paper uses the method applied in [6] to compute the ApEn.

$$ApEn(m, r, \tau, N) = \Phi^{m}(r) - \Phi^{m+1}(r) \quad (6)$$

$$\Phi^{m}(r) = \frac{1}{N-(m-1)\tau}\sum_{i=1}^{N-(m-1)\tau} \log C_i^m(r) \quad (7)$$

Where r, the filter parameter value, is r=0.2*SD, SD is the standard deviation of the signal and $C_i^m(r)$ is the correlation sum.

Sample entropy: The sample entropy, SampEn, is a measure of complexity that can be easily applied to any type of time series data. It is conceptually similar to approximate entropy (ApEn), but SampEn does not depend on the data size as much as ApEn does (Lee, 2010).

Phase space reconstruction

Reconstruction based on derivative approach: The phase space dimension or reconstruction dimension, usually symbolized by letter *d* or *E*, is defined as the number of states that can be displayed in phase space. Phase space in d- dimensions will display a number of points *{x (n)}* of the system, where each point is given by:

$$\vec{x}(n) = [x(n), x(n+T), \ldots, x(n+(d-1)T)] \quad (8)$$

Where *n* is a moment in time of a system variable, and *T* is a period between two consecutive measurements of the variable. There is a problem with the phase space graphical presentation, if it has more

than three dimensions (Jovic and Bogunovic, 2007). Phase space reconstruction is a standard procedure when analyzing chaotic systems. It shows the trajectory of the system in time. Here the phase space reconstruction is obtained by a method based on derivatives approach (Packard et al., 1980) that is, by taking $\vec{x'}(n)$, $\vec{x''}(n)$,…etc.

Reconstruction based on the singular spectrum approach (SSA): SSA is a method of decomposition of time-series into the sum of a small number of independent components. The basic SSA algorithm has two stages: decomposition and reconstruction. The decomposition stage requires embedding and singular value decomposition (SVD). Embedding decomposes the original time series into the trajectory matrix; SVD turns the trajectory matrix into the decomposed trajectory matrices which will turn into the trend, seasonal, monthly components, and white noises according to their singular values. The reconstruction stage demands the grouping to make subgroups of the decomposed trajectory matrices and diagonal averaging to reconstruct the new time series from the subgroups that is, the concept of SSA consists of four steps: embedding, SVD, grouping, and diagonal averaging and all these steps mentioned in details (Yung, 2009).

Amplitude adjusted Fourier transform (AAFT)

The AAFT algorithm generates surrogate data set and this paper takes the same steps mentioned in Garfield et al. (2005) to create the AAFT for uterine EMG data. The idea is to first rescale the value in the original time series so they are Gaussian. Then the FT algorithm can be used to make surrogate time series which have the same Fourier spectrum as the rescaled data. Finally, the Gaussian surrogate is then rescaled back to have the amplitude distribution as the original time series.

Time reversibility

A time series is said to be reversible only if its probabilistic properties are invariant with respect to time reversal (Hassan et al., 2010). In this research a simple equation described in Hassan et al. (2010) is used to calculate the time reversibility T_R for a signal X:

$$T_R(\tau) = \frac{1}{N-\tau}\sum_{n=\tau+1}^{N}(X_n - X_{n-\tau})^3 \quad (9)$$

Where N is the signal length and in this paper we used $\tau=1$. Time irreversibility can be taken as a strong signature of nonlinearity.

Maximal Lyapunov exponent and correlation dimension

To calculate both parameters a practical method in Fele-Žorž et al. (2008) is used which is based on input data, represented in a phase space. The phase space is a construct which demonstrates or visualizes the changes of the dynamical variables of a system. For any time series, the phase space which is the same as original phase space of the system is reconstructed by using time-delayed samples as the coordinates of the new system.

The maximal Lyapunov exponent estimates the amount of chaos in a system and represents the maximal velocity with which different, almost identical states of the system, diverge (Fele-Žorž et al., 2008). Then the Lyapunov exponent can be calculated as the following equation as the maximum Lyapunov exponent, λ, is a measure of how fast a trajectory converges from a given point into some other trajectory:

$$\lambda = \lim_{t\to\infty}\lim_{\|\Delta y_0\|\to 0}\frac{1}{t}\log\frac{\|\Delta y_t\|}{\|\Delta y_0\|} \quad (10)$$

Where $||\Delta y_0||$represents the Euclidean distance between two states of the system at some arbitrary time t_0 and $||\Delta y_t||$ represents the Euclidean distance between the two states of the system at some later time t.

In chaos theory, the correlation dimension, D_{corr}, is a measure of the dimensionality of the space occupied by a set of random points, often referred to as a type of fractal dimension. It is proportional to the probability of the distance between two points on a trajectory being less than some r [8]:

$$D_{corr} = \lim_{r\to 0}\frac{\log(C(r))}{\log(r)} \quad (11)$$

Where $C(r)$ is the correlation integral.

Principal component analysis

PCA is an orthogonal linear transformation that transforms the original time series by projecting it to a new set of coordinates in order of decreasing variance. The transformation is by definition an optimum transformation in the least squares sense. This method reduces the dimension of the representation space to keep only the most important information represented in fewer dimension space domains (The iPredict website [Online], 2012).

The PCA is applied for the parameters (AAFT, derivative phase space reconstruction, SSA and DCT) to obtain only ten features from 24001, 24000, 23999 and 24001 features respectively. To explain why only 10 features are chosen, two notes must be taken in consideration. First, the principal component coefficients for a M×N matrix - where M is the number of patterns and N is the number of features- are a N×N matrix. Second, the condition for classifier pattern matrix construction is that the term and preterm signals must have the same number of features. An explanation example, a 150×24001 matrix is the PCA input obtained from applying the AAFT on the training term signals and a 19×24001 matrix from the training preterm ones. After applying the PCA, a 24001×24001 matrix is obtained from the term AAFT spectrum and a 24001×24001 matrix from the preterm one. Then we can take only the first ten most principal components that have the highest variance into the ANN pattern matrix.

Artificial neural network

An important step is the classification step and actually, in this research, three types of artificial neural network ANNs are used to reach best results. One of them is unsupervised learning method (Kohonen self-organizing network) (Goyal and Goyal, 2011) and the others are supervised learning methods (feed-forward back propagation network and trainable cascade-forward back propagation network) (Goyal and Goyal, 2011). Each one of the previous networks is used for linear and non-linear features separately and gives its own parameters to compare. In the research a training data of 150 term signals and 19 preterm ones are used in addition to testing data of 111 term signals and 19 preterm ones.

RESULTS AND DISCUSSION

For each classifier, some parameters can be calculated to evaluate its performance. These parameters are:

Table 1. Resulting values of the used classifiers (linear).

Used classifier	Resulting values			
	FP	***FN***	***TP***	***TN***
Kohonen	12	52	7	59
Feed-forward	19	0	0	111
Cascade-forward	19	0	0	111

Table 2. Comparison of calculated parameters for the three used classifiers (linear).

Used classifier	Calculated parameter				
	FPR	***FNR***	**TPR**	***TNR***	***ACC (%)***
Kohonen	0.17	0.88	0.12	0.83	50.7
Cascade-forward	0.15	0.00	0.00	0.85	85.3
feed-forward	0.15	0.00	0.00	0.85	85.3

$$FPR = \frac{FP}{FP + TN}, \quad FNR = \frac{FN}{FN + TP} \tag{12}$$

$$TPR = \frac{TP}{TP + FN}, \quad TNR = \frac{TN}{TN + FP} \tag{13}$$

$$ACC = \frac{TP + TN}{TP + TN + FP + FN} \tag{14}$$

Where *TP*, *TN*, *FP* and *FN* stand respectively for True Positive, True Negative, False Positive and False Negative values. The values of *FPR*, *FNR*, *TPR*, *TNR* and *ACC* stand respectively for False Positive Rate, False Negative Rate, True Positive Rate (Sensitivity), True Negative Rate (Specificity) and Accuracy.

In the linear method as shown in Table 1 the Kohonen network can recognize 59 signals from 111 and seven signals from 19 for term and preterm uterine EMG respectively while the feed-forward and the cascade-forward networks cannot recognize any preterm uterine EMG signal. From these values Table 2 can be created and it indicates that the Kohonen network has a low sensitivity (0.12) which is higher than the feed-forward and cascade-forward networks' sensitivities (0.00) and it also has high FNR (0.88) while it is the opposite for the other classifiers with no FNR (0.00). From these values, we can observe that no one of the three used classifiers can separate between term and preterm deliveries in a perfect way where the Kohonen network can recognize some of the preterm records but also it classifies many term records as preterm ones. On the other hand the feed-forward and the cascade-forward networks cannot recognize any preterm record although they classify all the term records correctly. Figure 2 shows the representation of the results on the ROC graph.

In the non-linear method as shown in Table 3, the Kohonen network can recognize 80 signals from 111 and nine signals from 19 for term and preterm uterine EMG respectively and the feed-forward network can recognize 107 signals from 111 and seven signals from 19 for term and preterm uterine EMG respectively while the cascade-forward networks can recognize 110 from 111 term signals and ten from 19 preterm ones. From these values, Table 4 can be created and it indicates that the Kohonen network has a low sensitivity (0.22) and high specificity (0.89) but it also has high FNR (0.78) while the feed-forward network has moderate sensitivity (0.64), high specificity (0.90) and low FNR (0.36).The cascade-forward network has high sensitivity (0.91) and high specificity (0.92) which are higher than the other used classifiers and it also has low FNR (0.09) and low FPR (0.08) which are lower than the others. From these values, we can observe that the cascade-forward network gives the best results where the Kohonen network can recognize some of the preterm records but also it classifies many term records as preterm ones. On the other hand the feed-forward network recognizes term and preterm records with lower errors than the Kohonen network but higher than these for the cascade-forward network. Figure 3 shows the representation of the results on the ROC graph.

In the additional linear method as shown in Table 5, the Kohonen network can recognize 77 signals from 111 and seven signals from 19 for term and preterm uterine EMG respectively and the feed-forward network can recognize 108 signals from 111 and five signals from 19 for term and preterm uterine EMG respectively while the cascade-forward networks can recognize 109 from 111 term signals and eight from 19 preterm ones. From the above values, Table 6 can be created and it indicates that the Kohonen network has a low sensitivity (0.17) and high specificity (0.87) but it also has high FNR (0.83) while the feed-forward network has moderate sensitivity (0.63), high specificity (0.89) and moderate FNR (0.37).

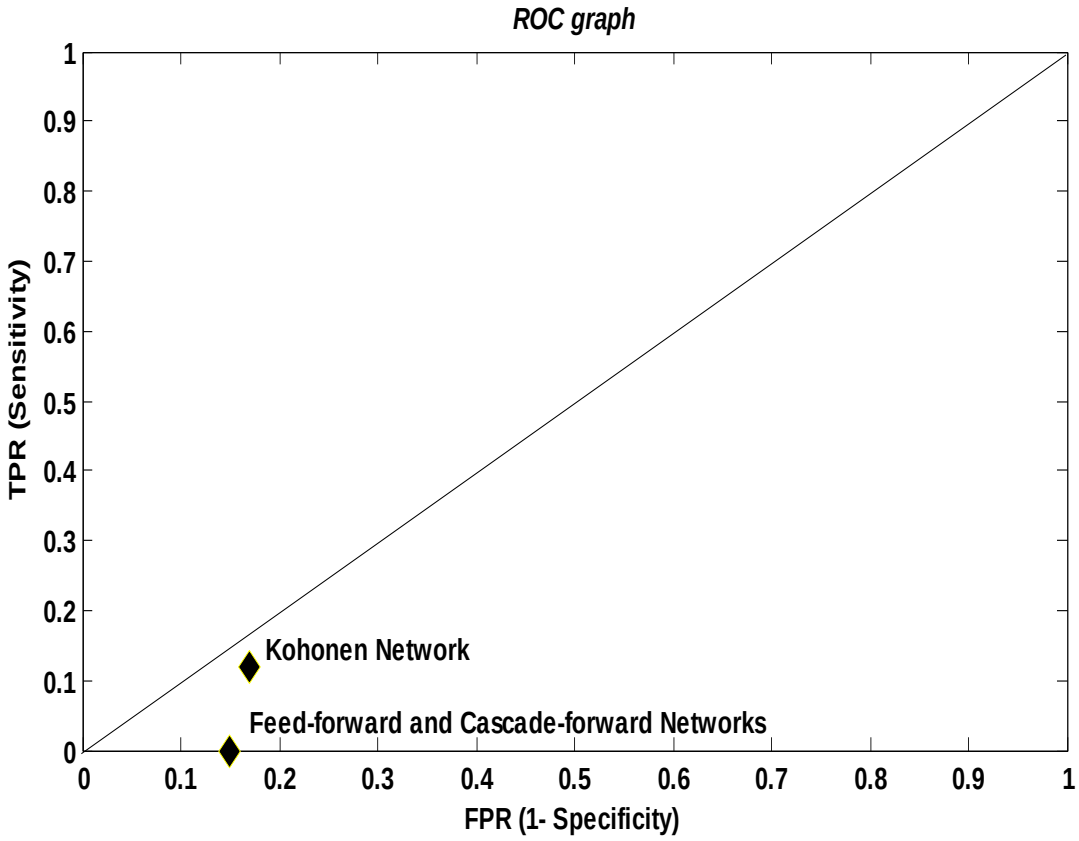

Figure 2. Representation of the results on ROC (Linear).

Table 3. Resulting values of the used classifiers (non-linear).

Used classifier	Resulting values			
	FP	***FN***	***TP***	***TN***
Kohonen	10	31	9	80
Feed-forward	12	4	7	107
Cascade-forward	9	1	10	110

Table 4. Comparison of calculated parameters for the three used classifiers (non-linear).

Used classifier	Calculated parameter				
	FPR	***FNR***	**TPR**	***TNR***	***ACC (%)***
Kohonen	0.11	0.78	0.22	0.89	68.5
Cascade-forward	0.10	0.36	0.64	0.90	87.7
Feed-forward	0.08	0.09	0.91	0.92	92.3

For the cascade-forward network, a sensitivity of (0.80) is obtained which is better than that in the previous linear method as it can recognize eight preterm signals from 19 ones and also it has low FNR (0.20) which is higher than that shown in Table 2 as it cannot recognize two term signals from 111 ones. In spite of that, the non-linear method shown in Table 4 is still the best. Figure 4 shows the representation of the results on the ROC graph.

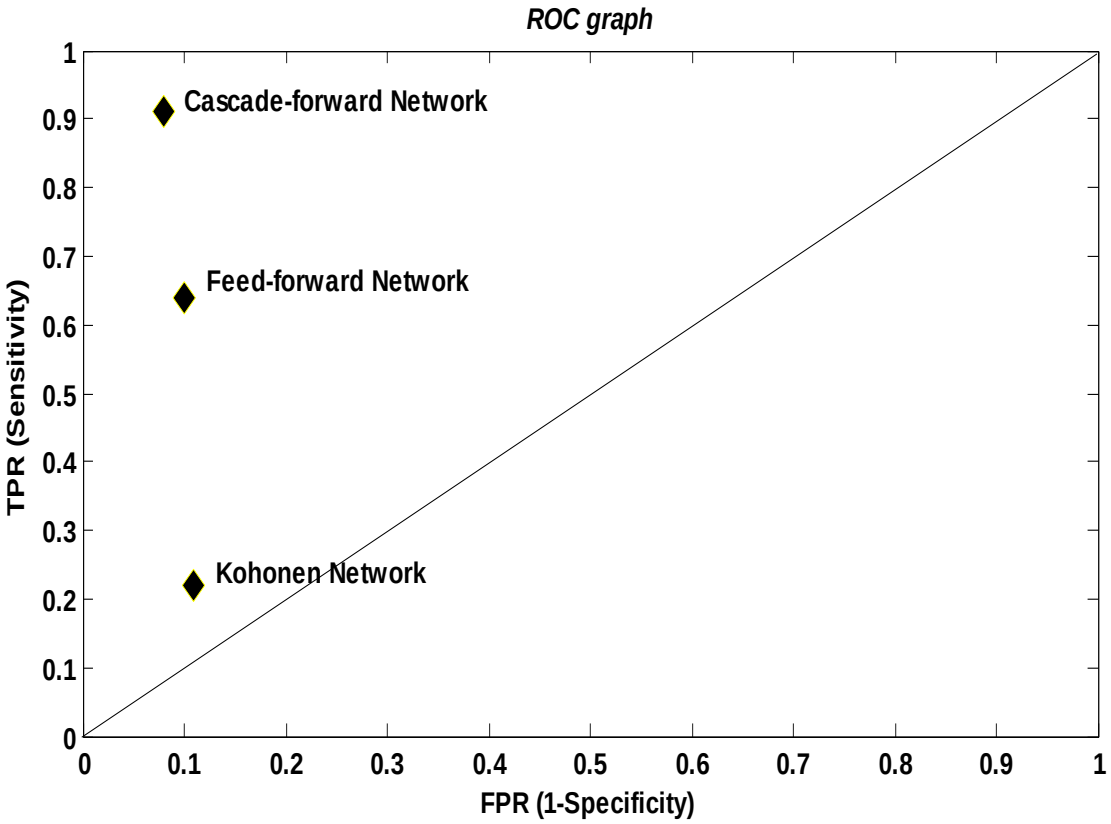

Figure 3. Representation of the results on ROC (Non- Linear).

Table 5. Resulting values of the used classifiers (linear+ DCT feature).

Used classifier	Resulting values			
	FP	***FN***	***TP***	***TN***
Kohonen	12	34	7	77
Feed-forward	14	3	5	108
Cascade-forward	11	2	8	109

Table 6. Comparison of calculated parameters for the three used classifiers (linear+ DCT feature).

Used classifier	Calculated parameter				
	FPR	***FNR***	**TPR**	***TNR***	***ACC (%)***
Kohonen	0.13	0.83	0.17	0.87	64.6
Cascade-forward	0.11	0.37	0.63	0.89	86.9
feed-forward	0.09	0.20	0.80	0.91	90

Conclusion

From the above results presented in this research some observations can be inferred. Firstly, using non-linear parameters of uterine EMG signals as ANN features can separate between term and preterm uterine EMG signals with results which are better than these for linear ones even if a spectral characteristic linear parameter (DCT) is used. Secondly, to get best classification accuracy with minimum error, you should use the trainable cascade-

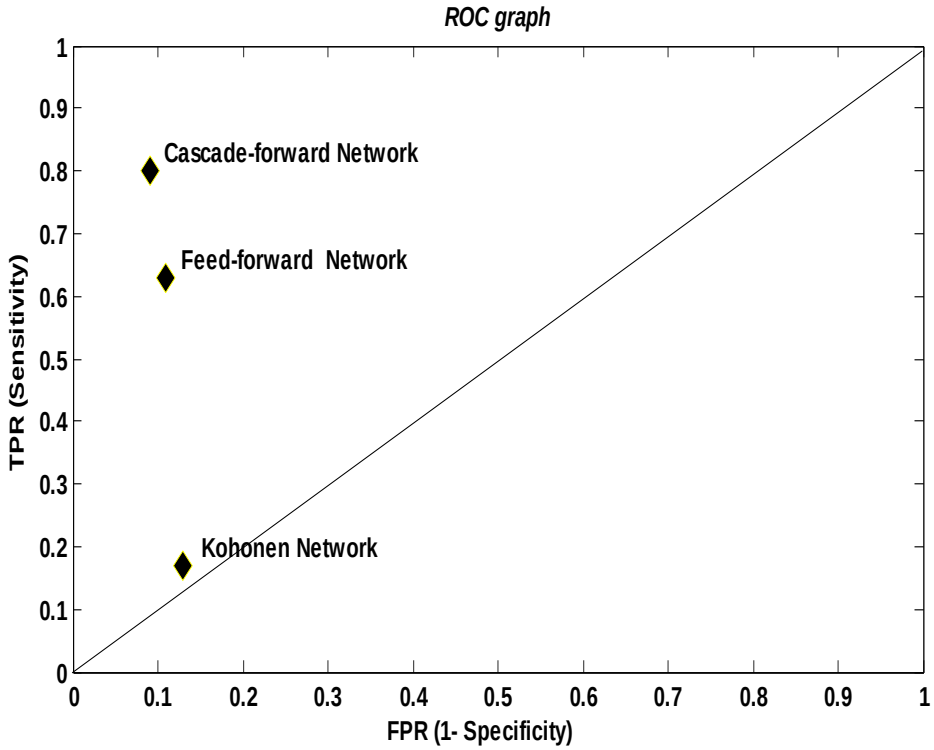

Figure 4. Representation of the results on ROC (Linear+ DCT feature).

forward back propagation network. Finally, the Kohonen network gives worse results in using both linear and non-linear parameters.

Conflict of Interest

The authors have not declared any conflict of interest.

REFERENCES

Diab MO, El-Merhie A, El-Halabi N, Khoder L (2010). "Classification of uterine EMG signals using supervised classification method. J. Biomed. Sci. Eng. 3:837-842.

Diab MO, Marque C, Khalil MA (2007). "Classification for Uterine EMG Signals: Comparison between AR Model and Statistical Classification Method," IJCC.

Moslem B, Diab MO, Khalil MA, Marque C (2012). "Combining data fusion with multiresolution analysis for improving the classification accuracy of uterine EMG signals," EURASIP J. Adv. Signal Proc. 2012.1 (2012):1-9.

Garfield RE, Maner WL, MacKay LB, Schlembach D, Saade GR (2005). "Comparing uterine electromyography activity of antepartum patients versus term labor patients." Am. J. ObstetGynecol, 193:23-29.

Maul H, Maner WL, Olson G, Saade GR, Garfield RE (2004). "Non-invasive transabdominal uterine electromyography correlates with the strength of intrauterine pressure and is predictive of labor and delivery," J Matern Fetal Neonatal Med. 15:297-301.

Hassan M, Terrien J, Alexandersson A, Marque C, Karlsson B (2010). "Nonlinearity of EHG signals used to distinguish active labor from normal pregnancy contractions," In Proceedings of the 32nd Annual International Conference of the IEEE EMBS: 31 August- 4 September 2010; Buenos Aires, Argentina.

Maner WL, Garfield RE (2007). "Identification of human term and preterm labor using artificial neural networks on uterine electromyography data," Ann. Biomed. Eng. 35:465-473.

Fele-Žorž G, Kavšek G, Novak-Antolič Z, Jager F (2008). "A comparison of various linear and non-linear signal processing techniques to separate uterine EMG records of term and pre-term delivery groups," Med. Biol. Eng. Comput. 46:911-922.

Akay M (2001). Nonlinear biomedical signal processing. In dynamic analysis and modeling, IEEE Inc. New York. 2.

Naeem SM, Ali AF, Eldosoky MA (2013). "Comparison between Using Linear and Non-linear Features to Classify Uterine Electromyography Signals of Term and Preterm Deliveries," In Proceedings of the 30th National Radio Science Conference NRSC: 16-18 April 2013; Cairo, Egypt. pp. 488-498.

Pincus SM (1991). "Approximate entropy as a measure of system complexity," Proc. Natl. Acad. Sci. U S A, 88:2297-301.

Lee K (2010). File exchange – Mathworks. [Online]. Available: http://www.mathworks.com/matlabcentral/fileexchange/35784-sample-entropy.

Jovic A, Bogunovic N (2007). "Feature extraction for ECG time-series mining based on chaos theory," In Proceedings of the ITI 29th Int. Conf. on Information Technology Interfaces: 25-28June 2007; Cavtat, Croatia.

Packard NH, Cruchfield JP, Farmer JD, Shaw RS (1980). "Geometry from a Time Series," Physical Rev. Lett, 45:712-715.

Yung NK (2009). Singular Spectrum Analysis, Master's Thesis. University of California, Los Angeles.

Nielsen F (2001). Neural Networks – algorithms and applications, Niels Brock Business College.

Goyal S, Goyal GK (2011). Cascade and Feed-forward Backpropagation Artificial Neural Network Models for Prediction of Sensory Quality of Instant Coffee Flavoured Sterilized Drink," Can. J. Artificial Intelligence, Mach. Learn. Pattern recognition.

academicJournals

Vol. 6(7), pp. 115-128, November 2014
DOI: 10.5897/JETR2013.0394
Article Number:ED7FC6848284
ISSN 2006-9790

http://www.academicjournals.org/JETR

Journal of Engineering and Technology Research

Full Length Research Paper

Applications of intelligent multi-agent systems for smart distribution systems

Yu-Hsiu Lin[1] and Men-Shen Tsai[2]*

[1]Graduate Institute of Mechanical and Electrical Engineering, National Taipei University of Technology, 1, Sec. 3, Zhongxiao E. Rd., Taipei 10608 Taiwan, R.O.C.
[2]Graduate Institute of Automation Technology, National Taipei University of Technology, 1, Sec. 3, Zhongxiao E. Rd., Taipei 10608 Taiwan, R.O.C.

Received 8 August, 2014; Accepted 9 October, 2014

Multi-agent systems (MAS) can be applied to service restoration planning of distribution systems. The main purpose of service restoration planning is to restore as many customers as possible. In this paper, a MAS-based service restoration planner with a Genetic Algorithm (GA) is developed to solve group and zone service restoration problems in power distribution systems. Intelligent software agents embedded inside switches and feeders of a distribution system form distributed MAS. They autonomously co-work in parallel, so that time consumption on service restoration planning is kept into minimum. By transferring de-energized customers to their adjacent supporting distribution feeders, the agents running autonomously and sharing information with each other restore out-of-service loads. The proposed methodology is implemented on a Java Agent Development (JADE) platform. The feasibility of the proposed MAS-based restoration planner is demonstrated by a distribution system.

Key words: Believe-Desire-Intension (BDI) agents, distribution systems, Java Agent Development (JADE), service restoration.

INTRODUCTION

In a typical distribution system/network, loads are partitioned by many switches. There are two types of switches: sectionalized (normally closed, N.C.) switches and tie (normally opened, N.O.) switches. The status of the switches must be properly regulated such that the radial network constraint of distribution systems is satisfied. Normally, the network topology can be re-configured. When an emergency occurs, power service to de-energized loads can be restored by service restoration plans. Several service restoration strategies have been proposed in Hsu et al. (1992), Tsai (2008), Chen et al. (2002), Parada et al. (2004), Huang (2003) and Kumar et al. (2008) with the following assumptions: 1) a centralized service restoration planner collecting all necessary information from fields is used; 2) the service restoration planning is based on combinatorial search; and 3) the switches are remotely controllable; that is, the service restoration planning made on the centralized service restoration planner can be executed remotely. However, massive data collected from a large-scale distribution

*Corresponding author. E-mail: mstsai@ntut.edu.tw.

system for service restoration need to be handled by the centralized service restoration planner. It results in high computational complexity and time complexity. As a result, a distributed intelligent Multi-agent system (MAS)-based service restoration planner is needed for service restoration, where intelligent agents co-work in a parallel fashion so that service restoration planning progresses more efficiently. Hence, the computational complexity and time complexity are de-centralized and reduced (it is not computationally expensive). Several MAS-based service restoration architectures have been used to solve service restoration problems (Nagata and Sasaki, 2002; Solanki et al., 2007; Pan and Tsai, 2011).

In Nagata and Sasaki (2002), a multi-agent approach to power system restoration was presented. In Solanki et al. (2007), a deliberative MAS was proposed. In Pan and Tsai (2011), a Believe-Desire-Intension (BDI) (Pan and Tsai, 2011; Bratman, 1999) based MAS that build a simple decision tree to identify the service restoration plans was proposed. However, the service restoration planning strategy is based on heuristics. In this paper, a distributed intelligent BDI- and MAS-based service restoration planner that plans service restoration strategies based on either heuristics or meta-heuristics by a Genetic Algorithm (GA) in a parallel manner is proposed. By gathering and analyzing information from other intelligent agents, each intelligent agent is capable of autonomously progressing for service restoration planning. The proposed MAS-based service restoration planner verified and validated by a distribution system provides group restoration service and zone restoration service to power system restoration. The experimental results confirm that the MAS-based service restoration planner proposed in this paper works well.

PROBLEM FORMULATION

When a fault happens in a distribution system, power service to customers may be interrupted. The goal of the service restoration planning is to restore power service to de-energized consumers as soon as possible. The service restoration problem can be formulated as follows:

$$Max \quad \sum_{i=1}^{n} x_i \cdot load_i \tag{1}$$

Where, $x_i = \begin{cases} 0, & \text{if the } i\text{-th zone is de-energized.} \\ 1, & \text{if the } i\text{-th zone is energized.} \end{cases}$

In Equation 1, n is the total number of zones. $load_i$ is the load of the i-th zone. The constraints of the service restoration problem solved in this paper include: 1) the line current of all conductors must not exceed the conductor capacity; 2) the distribution network must hold radial; and 3) the total load by each feeder must not exceed the feeder capacity. Besides, the distribution system considered in this paper has the following characteristics: 1) only the primary distribution feeder (11.4/22.8 kV) is considered; 2) three-phase laterals with switches connected to adjacent feeders are considered; and 3) three-phase currents are considered simultaneously.

METHODOLOGY FOR SERVICE RESTORATION PLANNING

The methodology for service restoration planning proposed in this paper is introduced here. In the proposed multi-agent architecture for the distribution system service restoration problems addressed in this paper, two different types of intelligent agents are defined.

1) Feeder agents: Feeder agents only respond to a query for the feeder ampacity. With responding to a query, they provide total served load current information and present available ampacity information. Each feeder agent maintains the information of exactly one adjacent switch that is directly connected to it (the feeder). Feeder agents do not make any service restoration planning.

2) **Switch agents:** Each switch agent, who records the current through the switch, is responsible for monitoring and controlling the status of the switch it is located at. This type of intelligent agents responds to queries from other intelligent agents. The topological information of adjacent intelligent agents of each intelligent agent is held by each switch agent. Adjacent intelligent agents can directly exchange their information. To gather more necessary information from non-adjacent intelligent agents, the adjacent intelligent agents have to rely on a message passing mechanism. Whenever a fault is detected and isolated occurs, switch agents start to plan the service restoration strategies.

Flowchart of the proposed self-healing approach

Figure 1 shows the flowchart of the proposed service restoration planning. The restoration planning starts when a fault detected occurs. Whenever a fault occurs, intelligent agents that belong to switch-type agents and are responsible for service restoration planning are identified and are named Leader Agents (LA) first. As soon as the LA(s) is identified, it starts communicating and interacting with other intelligent switch and feeder agents to explore the whole out-of-service (outage) area enclosed by the tie switches (within the tie switches). When all related information such as the available capacity of feeders is identified through a query process, the Las start planning service restoration strategies.

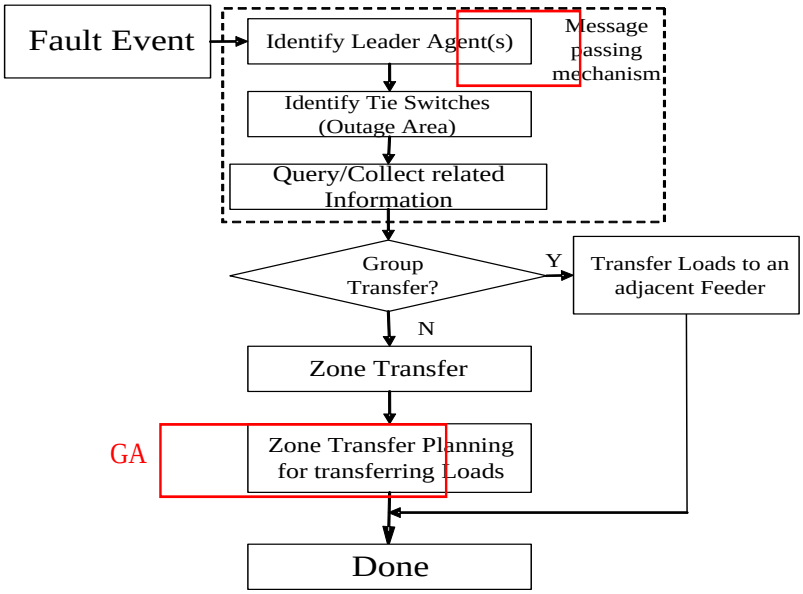

Figure 1. Flowchart of the self-healing strategy proposed in this paper.

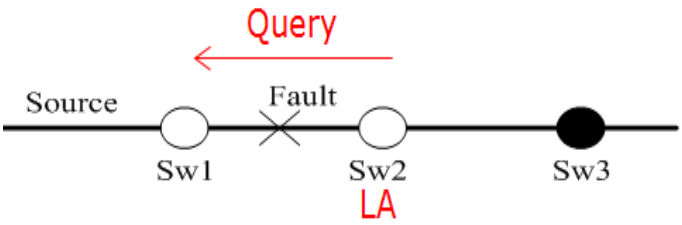

Figure 2. Occurrence of fault between two switches.

Finally, to restore power service to de-energized customers, intelligent agents perform necessary actions.

Message passing mechanism and service restoration planning

The message passing flow and the service restoration planning are discussed as follows:

Stage 1): Elect the LAs for service restoration planning

When a fault occurs, the status of the switches that surround the faulted section is marked "LOCKED_OPEN." When the intelligent agents installed inside the switches detect the change of the status, queries toward the power source side are sent by the intelligent agents. If the switch agent that received the query responds with "LOCKED_OPEN," the intelligent agent that sent the query is elected as the LA. The main goal of the LA(s) is to make an adequate service restoration plan based on the retrieved information from other agents. For example, suppose that a fault occurred between Sw1 and Sw2, as shown in Figure 2, the status of the two switches is set to "LOCKED_OPEN." Messages from Sw2 and Sw1 are sent toward the power source side. In this case, Sw2 is elected as the LA. If the fault is surrounded by more than two switch agents as shown in Figure 3, messages from Sw2, Sw4, and Sw1 are sent towards the power source side. Since the source of Sw2 and Sw4 is Sw1 and the status of Sw1 is "LOCKED_OPEN", both switch agents, Sw2 and Sw4, are elected as the LAs. The two LAs co-work for service restoration planning in a parallel manner, such that the time consumption on service restoration planning is improved.

Stage 2): Acquire necessaries for the outage area

The LAs send a query (queries) toward the down-stream sector, in order to identify all tie switches within the outage area. When a switch agent receives the query, it responds the topology and loading information to the LA.

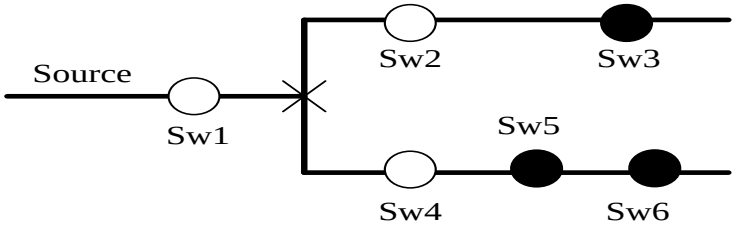

Figure 3. Occurrence of fault surrounded by three switches. In this situation, Sw2 and Sw4 are elected as the LAs; the service restoration strategies by the two LAs are separately and simultaneously planned (in a parallel way). Similarly, the service restoration strategies are planned by LAs in parallel such that the computational complexity and the time complexity are distributed and reduced, if there are multiple faults that occurred (at the same time) in a distribution system.

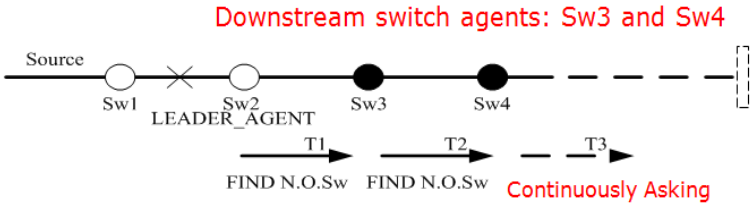

Figure 4. Search for tie switches.

If the status of the switch agent is not open, the query is continually passed to the switch agent's downstream switch agent(s). For example, as shown in Figure 4, the LA, Sw2, sends a query to the downstream switch agent, Sw3. Since the status of Sw3 is not open, the switch agent passes the query to its downstream switch agent. In the meantime, it also passes the topology and loading information to the LA. The query process is continued until a tie switch or the feeder is met. As shown in Figure 5, when a tie switch is queried, it responds its identity to the leader agent. If the number of downstream switch agents of a switch agent is more than one, the query is passed to the downstream switch agents. A special message "a branch has been identified" is sent to the LA. Thus, the LA is able to keep track of the number of branches that exist at its downstream sector. When all the tie switches send their identity to the LA, the search process terminates.

Stage 3): Identify the available ampacity of adjacent feeders

The intelligent agent located at the tie switch found in *Stage 2* sends the feeder capacity query message to its source-side intelligent agent. If the intelligent agent that receives the message is a feeder agent, it responds with the available capacity information to the tie switch agent; otherwise, it passes the query message to its source-side intelligent agent until a feeder agent is met. Finally, the adjacent feeder's available capacity information is sent to the LA. Figure 6 shows the search process.

Stage 4): LA(s) starts planning service restoration strategies

When all the related information is retrieved, the LA(s) starts planning service restoration strategies as follows:

Group restoration planning: The margin of one of all the adjacent feeders is sufficient enough for fully supporting all the de-energized customers in the out-of-service area.

Zone restoration planning: The zone restoration planning process starts when the group restoration planning process fails to restore all de-energized customers in an outage area(s). The zone restoration planning is composed of a heuristic approach and a GA. The GA is triggered for service restoration planning, when the heuristic approach is not able to identify an adequate service restoration plan. The heuristic approach is based on the Maximum capacity principle. During the service restoration planning, outage areas that are adjacent to the feeders are energized by the feeders. The feeders' available capacity is updated. Then, the power service to the rest of the areas is restored in turn by the feeder with the maximum available capacity at the current run. It progresses until each feeder' available capacity is not

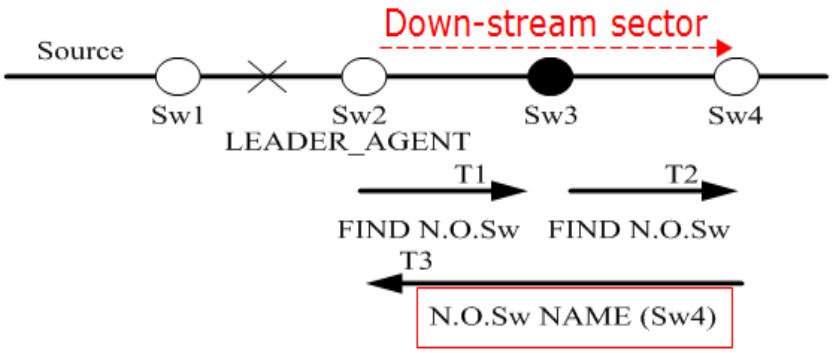

Figure 5. Information response from a tie-switch agent.

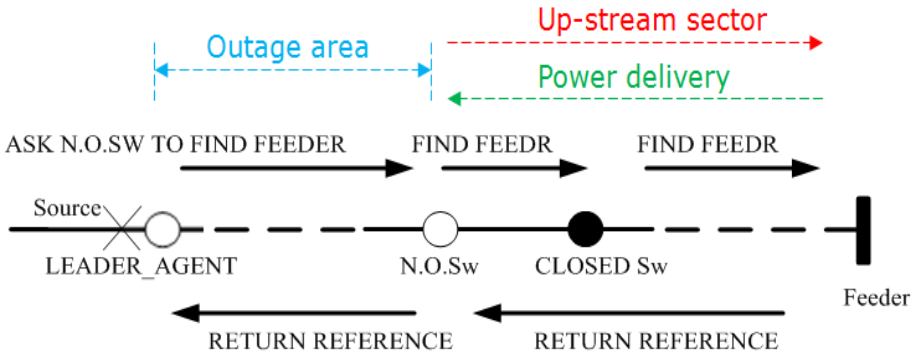

Figure 6. Search for an adjacent feeder.

sufficient for supporting the area that is located at the downstream sector of the feeder. In some cases, the heuristic approach is not able to restore power service to all de-energized zones. As a result, the population-based stochastic GA (Gen and Cheng, 1997) is conducted. It globally searches for the optimal network topology. With use of the GA planning service restoration strategies, one of the most important steps is to encode network topologies as chromosomes (genotype). Each gene, a binary number (0: Opened/1: Closed), of a chromosome presents the status of a switch on a feeder. To evaluate the quality of each chromosome, a fitness function, which guides the GA to search for the optimal solution, is needed. Since the service restoration to all de-energized zones is the final goal, the fitness function is defined as (1). During evaluation, the GA decodes each chromosome into the corresponding network topology (phenotype), checks whether the constraints are satisfied or not, and evaluates the fitness of each legal chromosome. The constraints have been mentioned earlier. If any violation exists, the reject mechanism that deletes the illegal ones is performed. After all legal chromosomes in the current population are evaluated, the natural (roulette wheel) selection process that mimics the process of Darwinian evolution to create populations from generation to generation is performed. The genetic operators facilitate an efficient search and guide the search into new solution regions. One-point crossover and bit-wise flipping mutation operators are used in this paper.

EXPERIMENTATION

The proposed MAS-based service restoration planner with the GA in this paper is implemented on the Java Agent Development (JADE) platform (Bellifemine et al., 2007) which is a platform for developing MASs and running the agents. It complies with the Foundation for Intelligent Physical Agents (FIPA) standards (Zidan and El-Saadany, 2012; Nguyen and Flueck, 2012). FIPA is an IEEE Computer Society Standards Organization, which promotes agent-based technology and the interoperability of its standards with other technologies. A test distribution system used to demonstrate the feasibility of the proposed multi-agent approach using the object-oriented design is shown in Figure 7. The distribution system is constructed by 9 feeders with 43 switches. In this paper, three different scenarios were simulated. During the experimentation, the following two assumptions are made:

1) The distribution systems with load variations are not covered; and
2) All load zones (customers) to be restored have the same load priority.

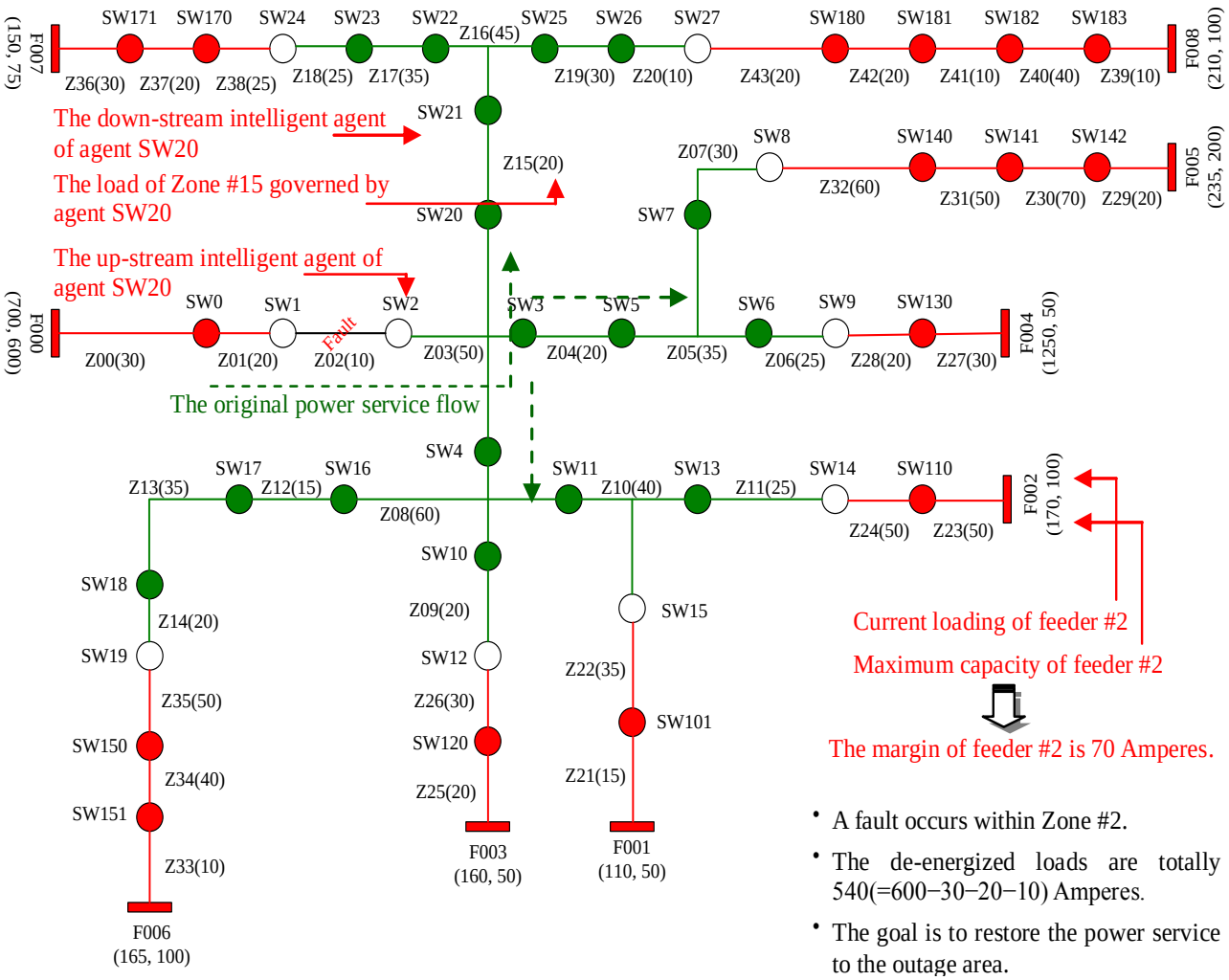

Figure 7. A large-scale distribution system used during the experiments conducted in this paper.

In Simulation 1, a fault occurred between Sw1 and Sw2 (within zone Z02). The leader agent elected was Sw2. In this simulation, the de-energized loads are totally 540 A. The goal is to restore the power service to the whole outage area shown in green color in Figure 7. According to the network typology shown in Figure 7, intelligent switch agents and feeder agents are set up as shown in Figure 8. Figure 9 shows the JADE remote agent management GUI showing the set-up intelligent switch agents and feeder agents. Figure 10 shows the message passing and querying process. The interaction of intelligent switch and feeder agents leads to a dynamic and effective system allowing an efficient service restoration to a solution. Intelligent switch agents and feeder agents exchange information and autonomously co-work in a parallel fashion so that the service restoration planning progresses more efficiently. The outage area in this simulation is finally figured out through the message passing mechanism. The group restoration result obtained in this simulation is reported in Figure 11. The margin of feeder #4 (F004) was very sufficient for supporting all the out-of-service zones in the outage area. Hence, the LA, Sw2, made a decision that Sw9 is switched on; the group restoration was made, where all the de-energized customers were served. The computational time is less than 10 s. Figure 12 shows the finally-configured topology of the distribution system. No any constraint was violated and the goal was achieved.

In Simulation 2, the heuristics-based zone restoration planning process is executed by the MAS proposed in this paper for service restoration planning, since the margin of one of all the adjacent feeders is not sufficient enough for fully supporting the out-of-service customers in the outage area as seen in Figure 13(a). The message passing mechanism has been presented earlier. Also, based on the heuristic-based zone restoration planning strategy-Maximum capacity principle introduced earlier, the MAS fully restore a total of 540 Amperes. During the service restoration process, all the constraints are satisfied. The computational time is less than 10 s. The final topology of the distribution system is shown in Figure 13(b).

In Simulation 3, the GA-based zone restoration planning where switches in a distribution system are encoded and evolved through the genetic operations-crossover and mutation and the evolution operation-selection was adopted by the proposed MAS, because the heuristics fail in this case. The GA globally searches for the optimal network topology. The distribution system tested is illustrated in Figure 14. The message passing mechanism and the meta-heuristic-based zone restoration planning strategy by a GA

Figure 8. Intelligent switch agents for planning service restoration strategies and intelligent feeder agents are set up (through a *.bat file).

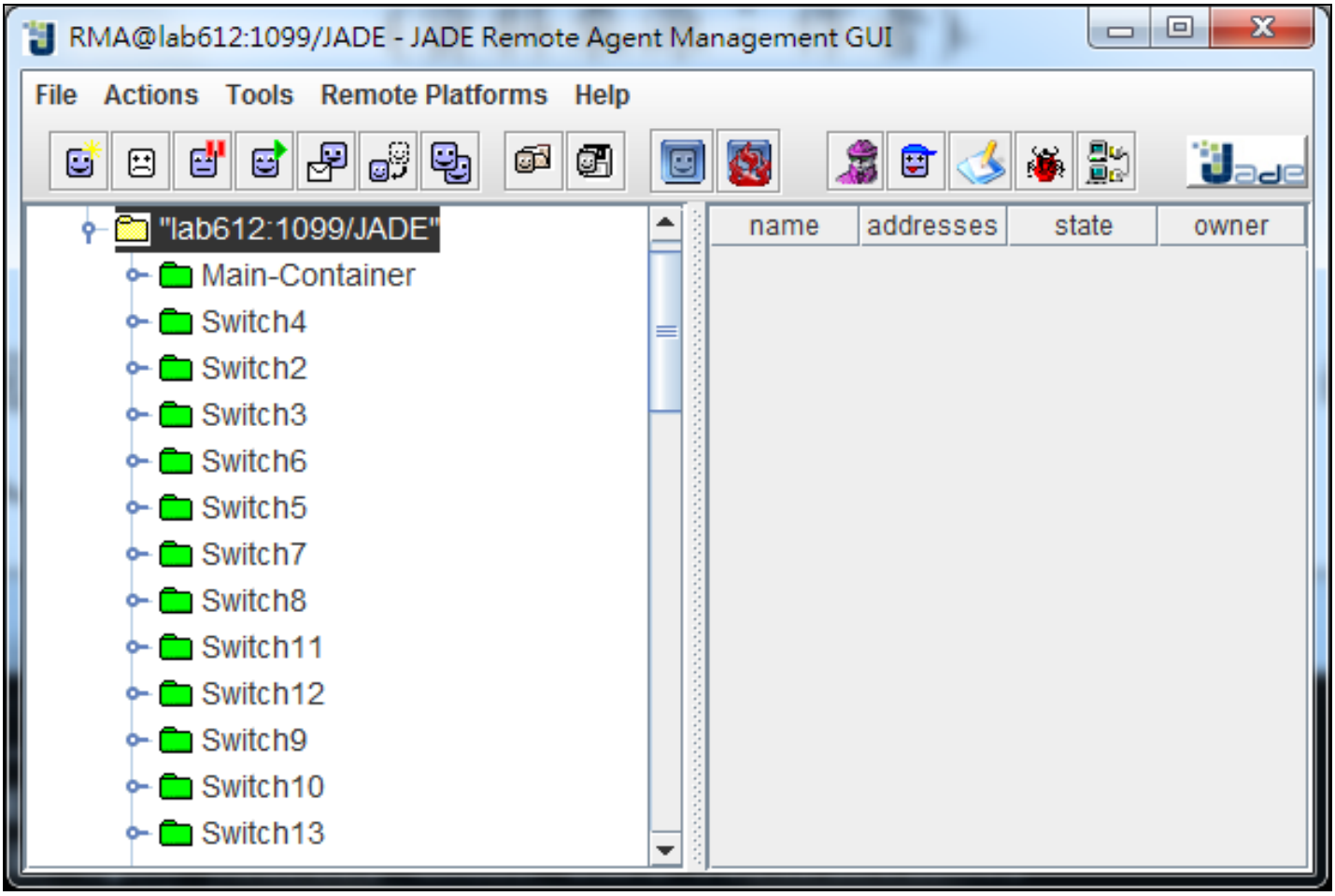

Figure 9. JADE remote agent management GUI showing the set-up intelligent switch agents and feeder agents. The Remote Monitoring Agent (RMA) is a graphical console to monitor the agent platform activity and visualize container and agent states. The number of switch agents/feeder agents is the same as the number of switches/feeders in a distribution system. Intelligent agents in JADE communicate by the message passing mechanism, where the messages adhere to Agent Communication Language (ACL) standards.

have been presented earlier. For the GA, the population size is 20. The maximum generation is 10; and the crossover rate and the mutation rate are 0.45 and 0.05, respectively. Figure 15 shows the evolution by the GA. The computational time is less than 10 s. The final topology of the distribution system re-configured by the proposed MAS in this simulation is shown in Figure 16. As shown in Figure 16, 3 out-of-service zones, Z3 (load: 50), Z4 (load: 20) and Z8 (load: 60), existed. ~75.93 of power service (410 of 540 A) was served. The search accuracy/efficiency of the GA employed in this simulation is improvable.

For this service restoration problem, the legal solutions are finite. For the encoding method used by the GA, most of the offspring generated by the genetic operators are illegal. A lot of time is wasted, due to the large number of illegal solutions. If an appropriate encoding method is conducted, the search accuracy/efficiency of the GA can be improved. And, the power service to all the outage areas can be fully restored.

Conclusions

This paper presents a completely distributed MAS-based service restoration planner with the heuristics and the GA for distribution systems service restoration problems. Compared with the centralized one, the proposed MAS-based service restoration planner has several advantages. For instance, service restoration planning is made in a parallel fashion. The experimentation reported in this paper shows that the proposed distributed MAS-based service restoration planner using the agent- and object-oriented design and reporting the adequate service restoration plan is feasible. The quality of service restoration planning is improved. This is because the MAS is conducted to the smart distribution systems. In a MAS, each intelligent agent merely collects local information, while communicating and interacting with other intelligent agents to figure out the whole outage area(s). Then, the service restoration planning to a large-scale distribution system that suffers from at least one fault (multiple faults may occur) can be de-centralized into a series of sub-tasks (it can be tackled in a divide-and-conquer manner).

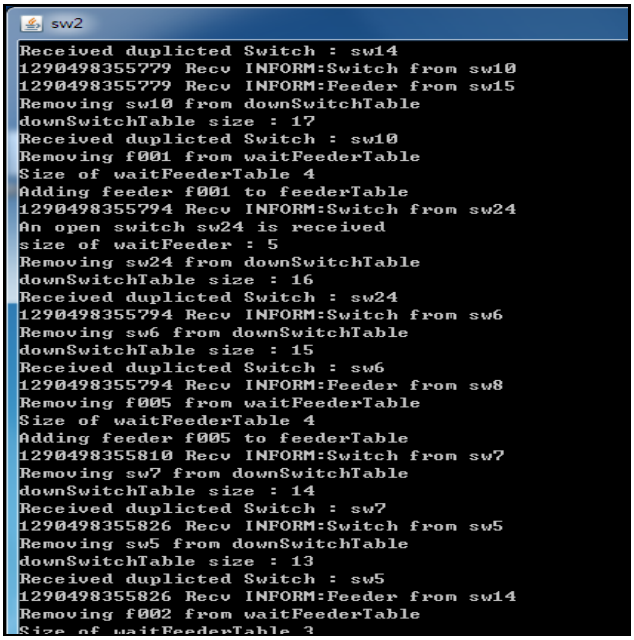

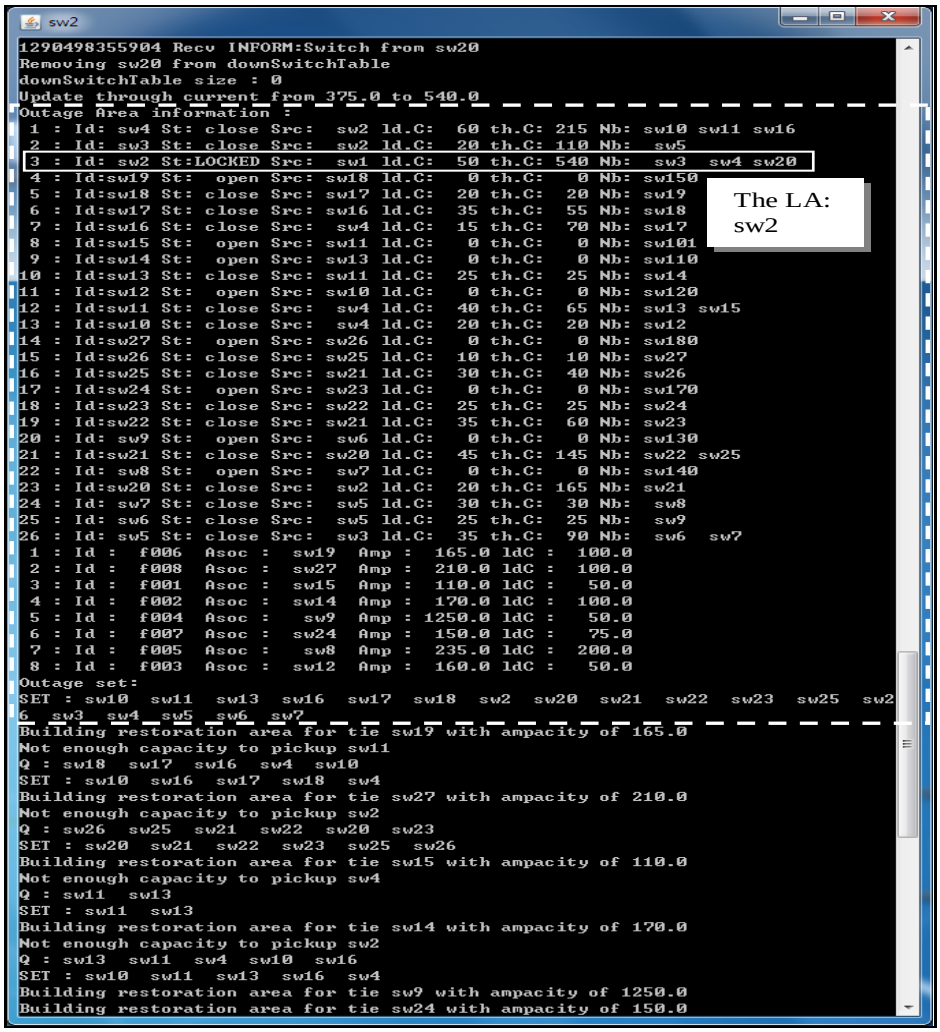

Figure 10. Message passing and querying. The outage area information is collected through the message passing mechanism.

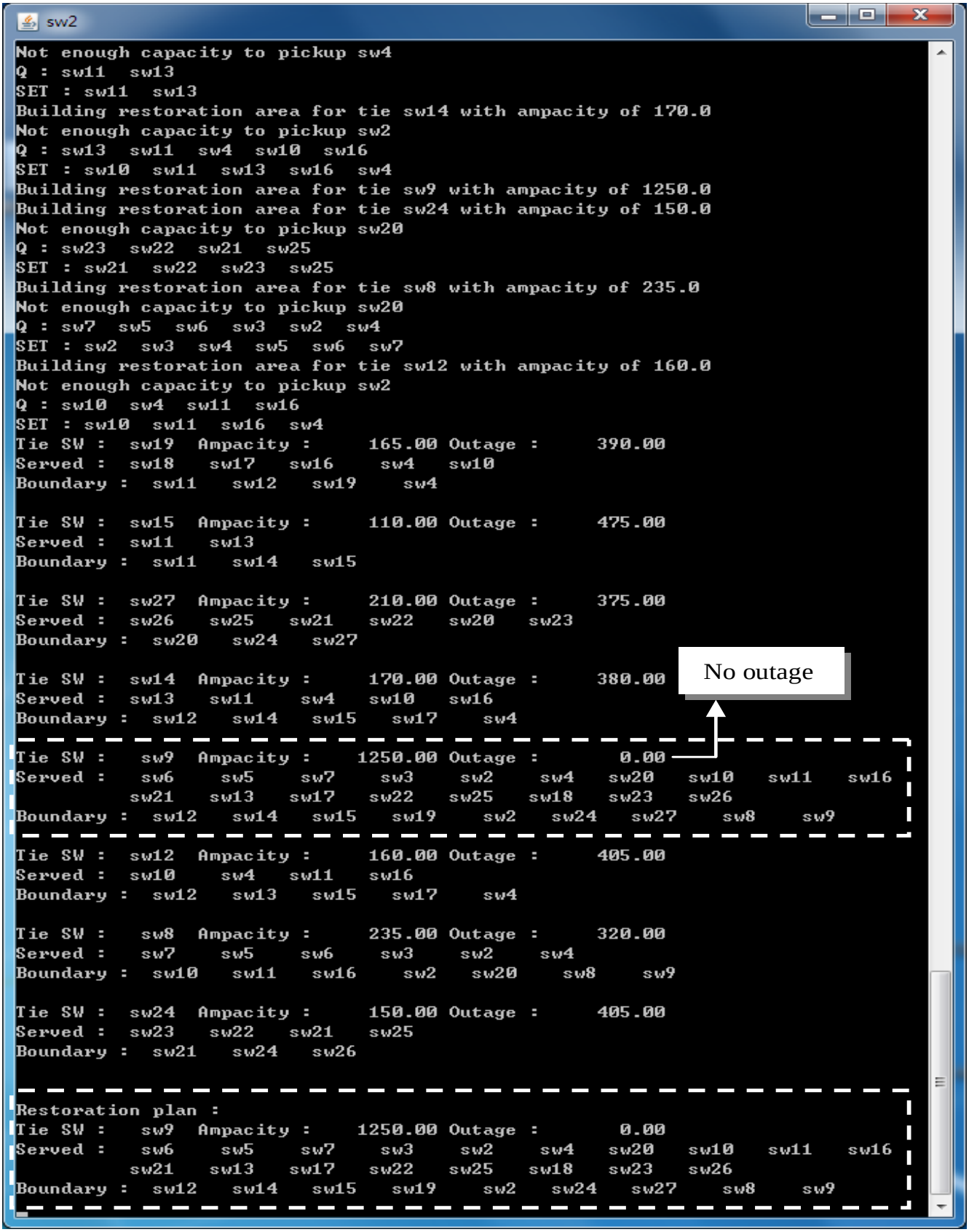

Figure 11. Group restoration result in this simulation. The message passing mechanism and the group restoration planning strategy is presented in the work. The group restoration decision was made, where all the de-energized customers were served.

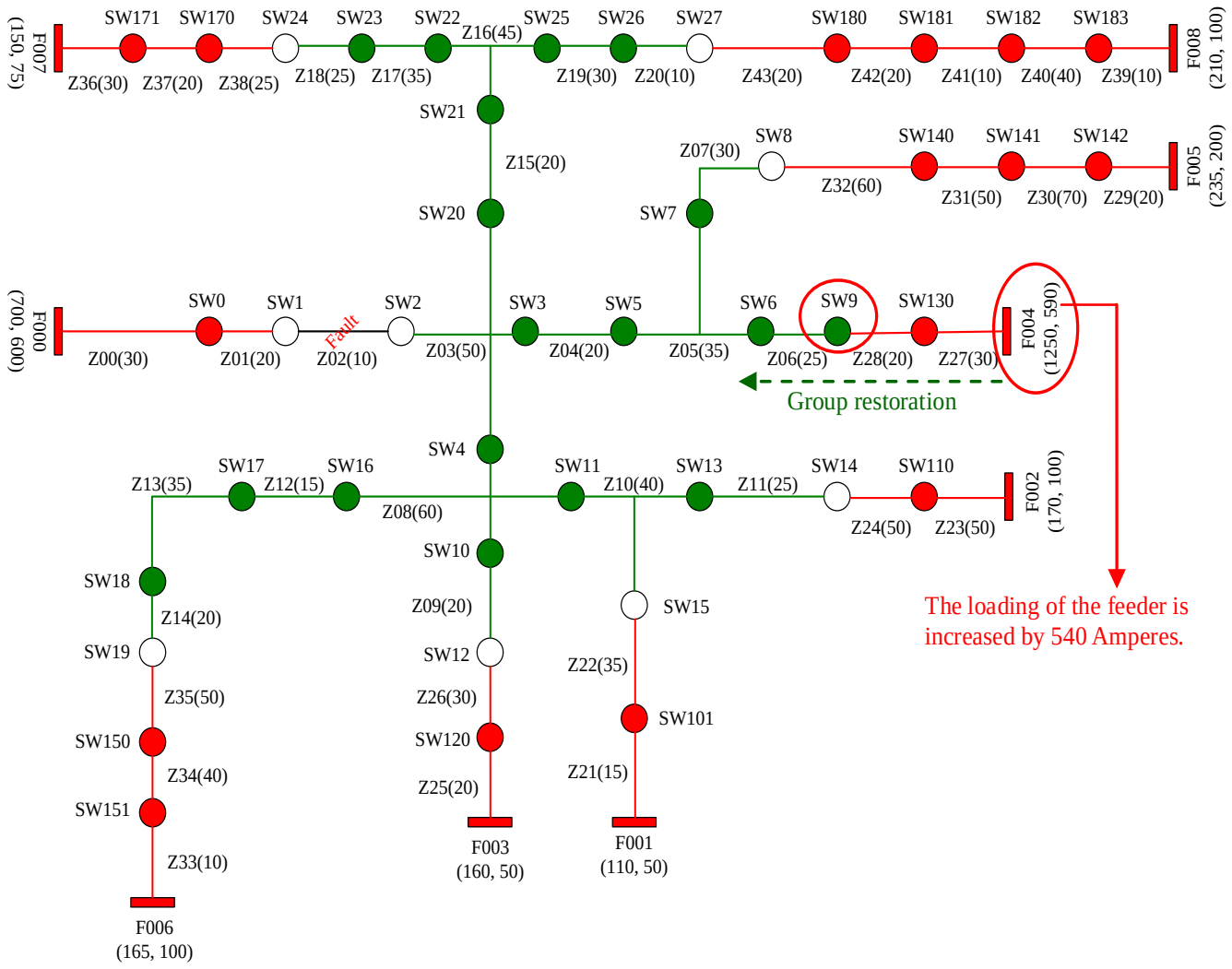

Figure 12. The finally-configured network topology of the distribution system given in Figure 7 in this simulation is obtained through the self-healing process by the proposed MAS. The network topology is re-configured through *switching*. In this simulation, the margin of F004 was very sufficient for supporting all the out-of-service zones.

With a parallel, asynchronous, and autonomous process of planning service restoration strategies, the computational complexity and the time complexity are distributed and reduced. Besides, the MAS have a high degree of scalability and flexibility. Overall, for fault detection and isolation and service restoration, a de-centralized multi-agent framework could outperform the centralized ones requiring a powerful central computer that may lead to a single point of failure.

In the future, if an appropriate encoding method is conducted, the search accuracy and efficiency of the GA can be improved. It is expected that the power service to all de-energized consumers in an outage area(s) is fully restored. The next step of this work is to improve the performance of the MAS proposed in this paper, in order for coping with the difficulty in self-healing distribution systems under multiple faults. The enhanced MAS will be a promising approach to more complex large-scale distribution networks that suffer from multiple faults.

ACKNOWLEDGEMENTS AND LEGAL RESPONSIBILITY

This paper was supported in part by the National Science Council, Taiwan, under the Grant No. NSC 101-2221-E-027-097-MY2- and MOST 103-3113-E-006 -011, and was sponsored in part by the Ministry of Education (MOE) with Technological University Paradigms, Taiwan, under the Grant No. 7021401-4. This study is an original work that has neither appeared elsewhere for publication, nor which is under review for another refereed publication.

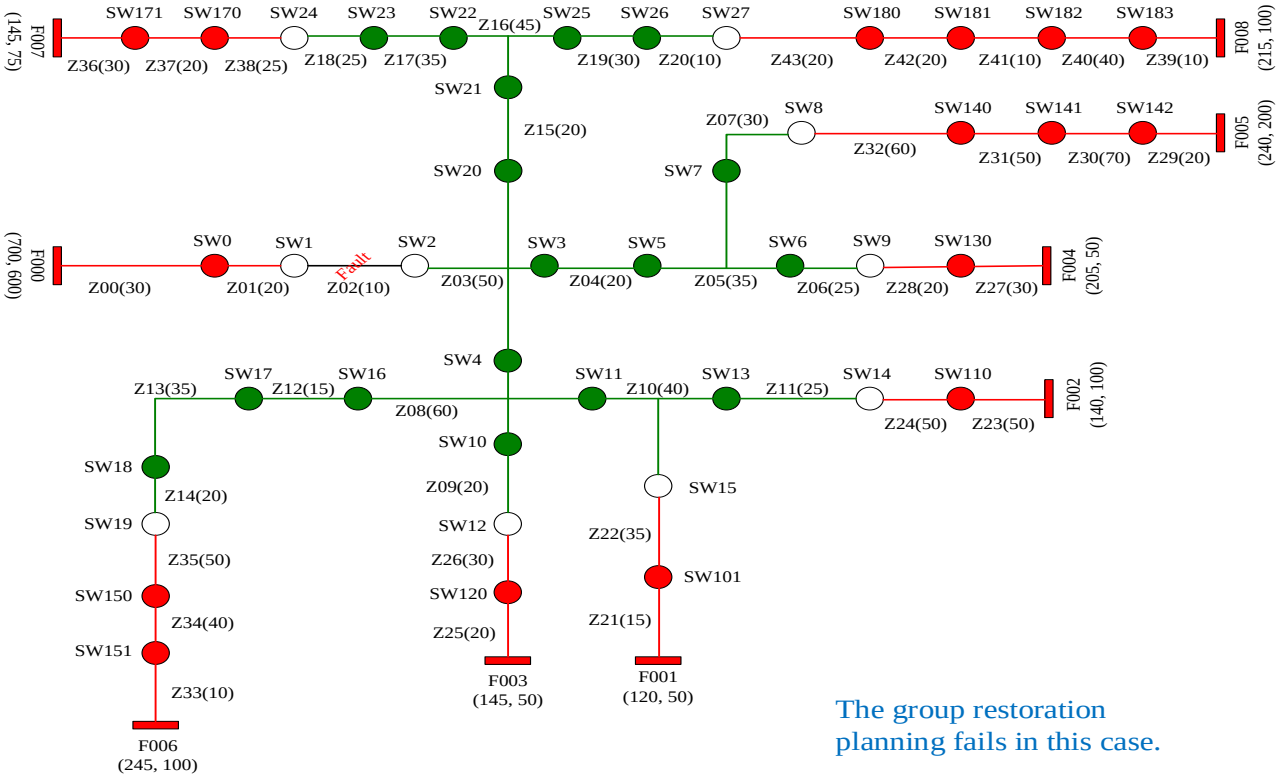

(a)

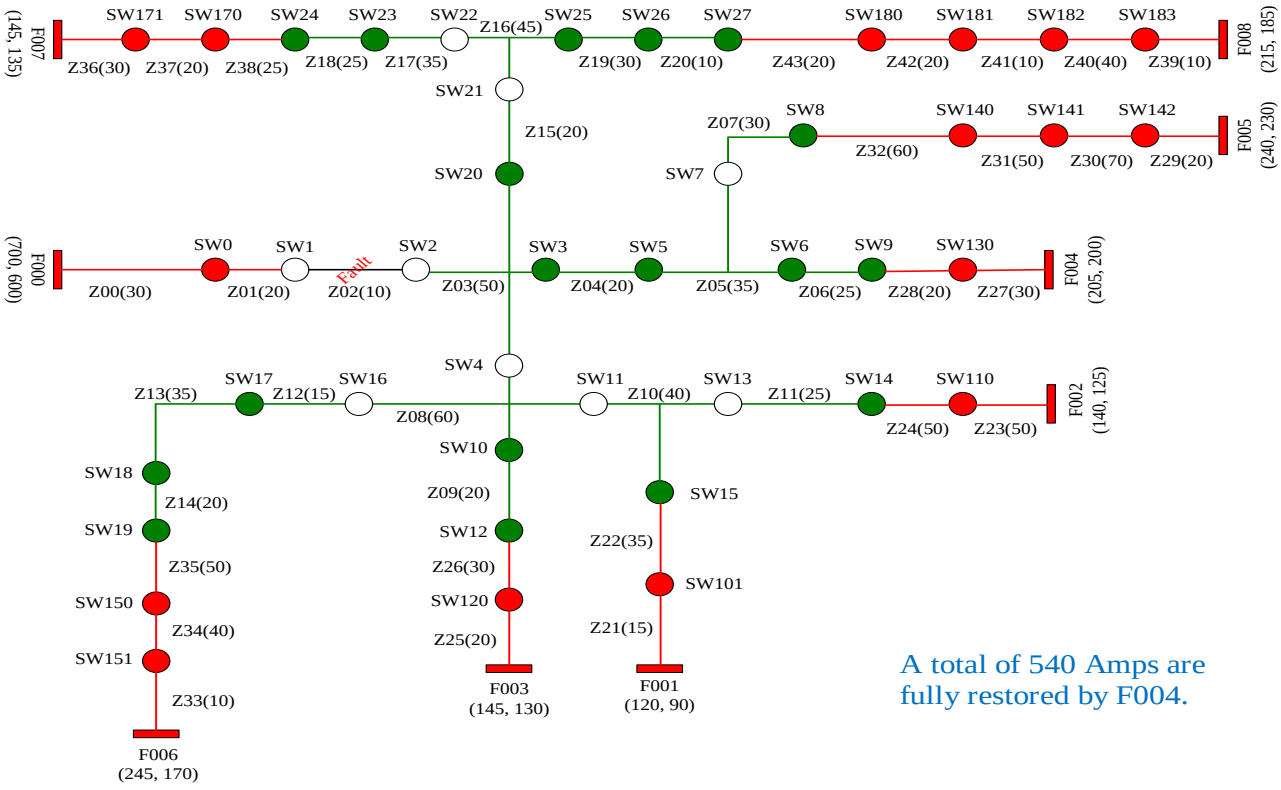

(b)

Figure 13. A large-scale distribution system used in Simulation 2 (a) and the final topology configured by the proposed MAS for power service restoration (b).

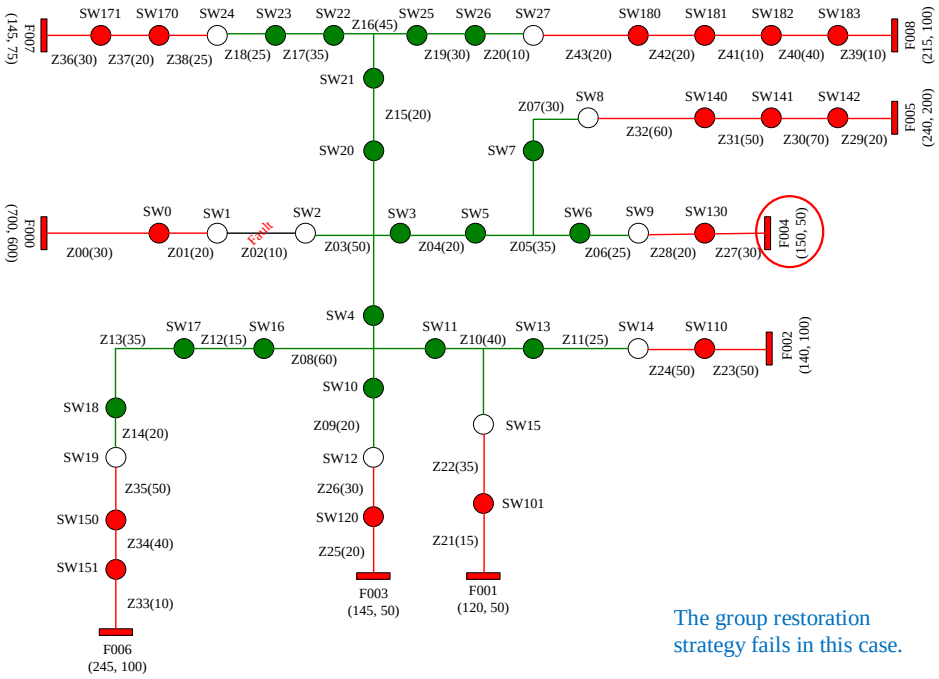

Figure 14. A large-scale power distribution system used in Simulation 3.

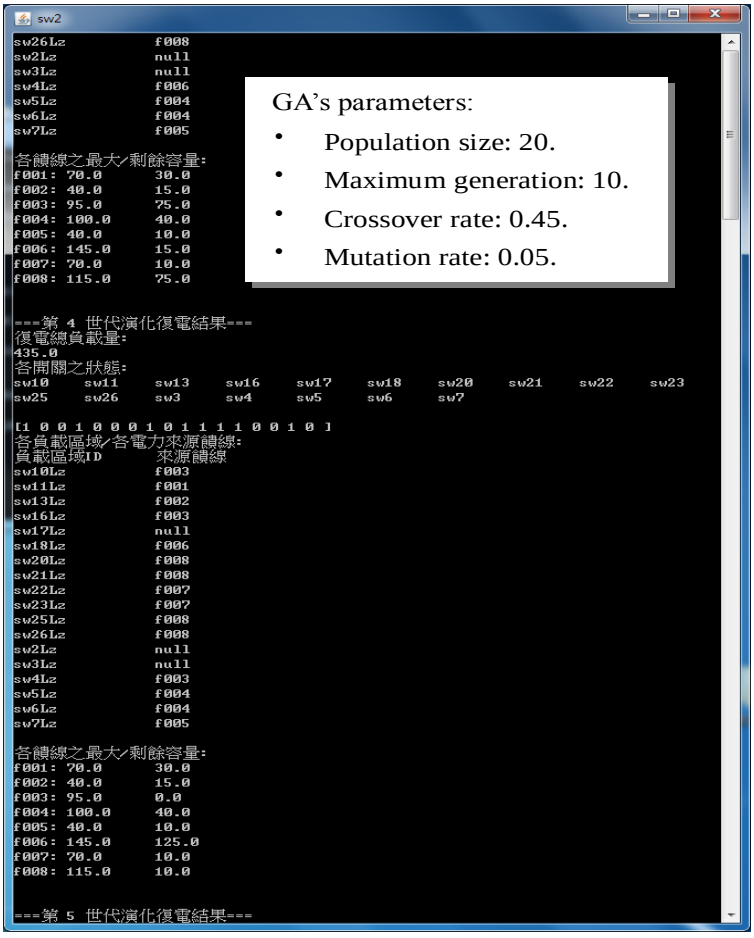

Figure 15. Evolution by the GA.

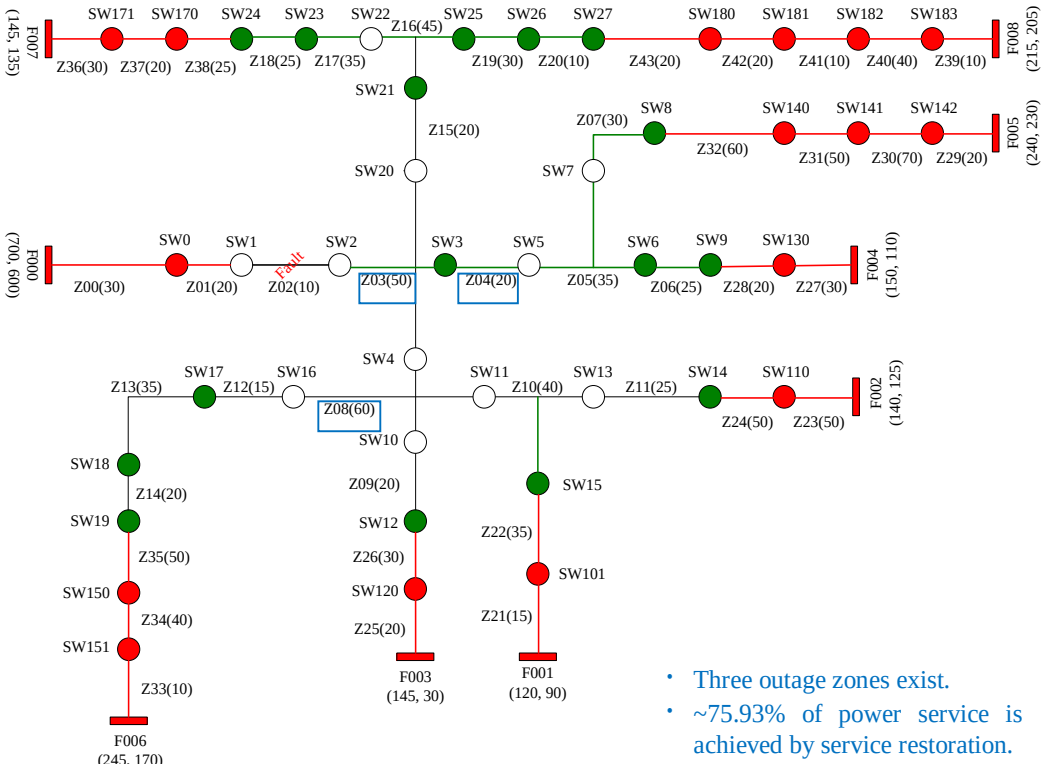

Figure 16. The finally-configured topology obtained by the proposed MAS for power service restoration in this simulation.

Conflict of Interest

The author(s) have not declared any conflict of interest.

REFERENCES

Bellifemine FL, Caire G, Greenwood D (2007). Developing multi-agent systems with JADE. Wiley.

Bratman ME (1999). Intention, plans, and practical reason. Harvard University Press: Cambridge, Massachusetts, USA.

Chen CS, Lin CH, Tsai HY (2002). A rule-based expert system with colored Petri net models for distribution system service restoration. IEEE Trans. Power Syst. 17(4):1073-1080.

Gen M, Cheng R (1997). Genetic algorithms and engineering design. Wiley-Interscience.

Hsu YY, Huang HM, Kuo HC, Peng SK, Chang CW, Chang KJ, Yu HS, Chow CE, Kuo RT (1992). Distribution system service restoration using a heuristic search approach. IEEE Trans. Power Deliv. 7(2):734-740.

Huang CM (2003). Multiobjective service restoration of distribution systems using fuzzy cause-effect networks. IEEE Trans. Power Syst. 18(2):867-874.

Kumar Y, Das B, Sharma J (2008). Multiobjective, multiconstraint service restoration of electric power distribution system with priority customers. IEEE Trans. Power Deliv. 23(1):261-270.

Nagata T, Sasaki H (2002). A multi-agent approach to power system restoration. IEEE Trans. Power Syst. 17(2):457-462.

Nguyen CP, Flueck AJ (2012). Agent based restoration with distributed energy storage support in smart grids. IEEE Trans. Smart Grid. 3(2): 1029-1038.

Pan YT, Tsai MS (2011). Application of BDI-based intelligent multi-agent systems for distribution system service restoration planning. European Trans. Elect. Power. 21(1):1783-1801.

Parada V, Ferland JA, Arias M, Daniels K (2004). Optimization of electrical distribution feeders using simulated annealing. IEEE Trans. Power Deliv. 19(3):1135-1141.

Solanki JM, Khushalani S, Schulz NN (2007). A multi-agent solution to distribution systems restoration. IEEE Trans. Power Syst. 22(3):1026-1034.

Tsai MS (2008). Development of an object-oriented service restoration expert system with load variations. IEEE Trans. Power Syst. 23(1):219-225.

Zidan A, El-Saadany EF (2012). A cooperative multiagent framework for self-healing mechanisms in distribution systems. IEEE Trans. Smart Grid. 3(3):1525-1539.

Journal of Engineering and Technology Research

Related Journals Published by Academic Journals

- *Journal of Chemical Engineering and Material Science*
- *International Journal of Water Resources and Environmental Engineering*
- *Journal of Civil Engineering and Construction Technology*
- *International Journal of Computer Engineering Research*
- *Journal of Electrical and Electronics Engineering Research*
- *Journal of Engineering and Computer Innovations*
- *Journal of Mechanical Engineering Research*
- *Journal of Petroleum and Gas Engineering*

academicJournals